



Review of the SAPRC-07 Chemical Mechanism

Merched Azzi, Stephen White, and Dennys Angove
ET/IR 1080
November 2008

Prepared for Dr Ajith Kaduwela
California Air Resources Board (CARB)

Enquiries should be addressed to:

Dr Merched Azzi

CSIRO Energy Technology

Phone: +61 2 9710 6870

Email: merched.azzi@csiro.au

Copyright and Disclaimer

© 2008 CSIRO To the extent permitted by law, all rights are reserved and no part of this publication covered by copyright may be reproduced or copied in any form or by any means except with the written permission of CSIRO.

Important Disclaimer

CSIRO advises that the information contained in this publication comprises general statements based on scientific research. The reader is advised and needs to be aware that such information may be incomplete or unable to be used in any specific situation. No reliance or actions must therefore be made on that information without seeking prior expert professional, scientific and technical advice. To the extent permitted by law, CSIRO (including its employees and consultants) excludes all liability to any person for any consequences, including but not limited to all losses, damages, costs, expenses and any other compensation, arising directly or indirectly from using this publication (in part or in whole) and any information or material contained in it.

Contact Us

Phone: 1300 363 400

+61 3 9545 2176

Email: enquiries@csiro.au

Web: www.csiro.au

Your CSIRO

Australia is founding its future on science and innovation. Its national science agency, CSIRO, is a powerhouse of ideas, technologies and skills for building prosperity, growth, health and sustainability. It serves governments, industries, business and communities across the nation.

CONTENTS

SUMMARY	5
1 INTRODUCTION.....	7
2 EXPERIMENTAL	8
2.1 Choice of Modelling Scenarios.....	9
2.2 <i>m</i> -Xylene.....	11
2.3 Toluene.....	19
2.4 Isoprene.....	22
2.5 ULP Experiments	25
3 CONCLUSIONS AND FURTHER WORK	30
4. ACKNOWLEDGEMENTS.....	31
5. REFERENCES.....	32
APPENDIX A: AUXILIARY MECHANISM	35
APPENDIX B: M-XYLENE EXPERIMENT RESULTS	40
APPENDIX C: ISOPRENE EXPERIMENT RESULTS	44

This page was intentionally left blank

SUMMARY

The performance of the SAPRC-07 chemical mechanism has been evaluated using the CSIRO smog chamber facility. The study assessed the capability of the model in reproducing ozone formation and the formation of other key species from the irradiation of different hydrocarbons with NO_x.

Two sets of smog chamber experiments were carried out to test the performance of the latest SAPRC-07 mechanism in terms of reproducing experimental results. The first set consists of a series of smog chamber experiments using reactive species with relatively well-known chemical reactions such as isoprene and *m*-xylene, and toluene for which the mechanism requires further development. The second set of experiments used wholly and partially evaporated unleaded petrol (ULP), hydrocarbon mixtures that are typical of urban emissions. Simulations of the complex hydrocarbon mixture/NO_x irradiations allowed for the overall performance of the mechanism to be evaluated for mixtures of hydrocarbons under controlled conditions. Three chemical mechanisms, SAPRC-07, SAPRC-99 and MCMv3.1, were used to simulate the smog chamber experiments and the simulated results for each mechanism were compared both to the other mechanisms and to available experimental data. The CSIRO smog chamber heterogeneous wall mechanism describing the chemical processes occurring on the chamber walls was updated for the current simulations.

The results predicted by the selected mechanisms can be summarised as follows:

For single compounds;

- SAPRC-07 predicted the ozone formation from *m*-xylene sufficiently well, with a slight improvement observed when compared to SAPRC-99 predictions and a more considerable improvement over MCM predictions. The onset of ozone formation was modelled slightly early for experiments containing higher initial ROC/NO_x ratios, whereas for low ROC/NO_x experiments the rate of ozone formation was slower than observed.
- The rate of isoprene degradation and initial ozone formation was well predicted for all models tested, however the mechanism failed to reproduce the timing and the magnitude of the transition from the hydrocarbon regime to the NO_x-limited conditions. This is believed to be related to the NO_y balance during this period, in particular the reactions of nitrogen-containing organic species.
- Oxidant formation from toluene was not well predicted by any model tested. SAPRC-07 in general predicted slightly better ozone profiles than SAPRC-99 or MCM, but the rate of ozone and other oxidant formation was much slower than observed for all experiments.

For wholly and partially evaporated ULP (gasoline);

- For wholly evaporated ULP, SAPRC-99 has predicted ozone formation and nitric oxide oxidation well. However SAPRC-99 also overestimated the hydrocarbon consumed during the experiment. SAPRC-07 underestimated ozone formation from wholly evaporated ULP when compared with SAPRC-99.
- For partially evaporated (headspace vapour) ULP, both SAPRC models predicted ozone formation well, as well as predicting VOC and NO oxidation accurately. However SAPRC-99 produced higher final ozone than SAPRC-07.

- The key difference between the wholly evaporated ULP vapour and headspace vapour experiments is that the concentration of aromatic species is significantly higher in the wholly evaporated ULP. This indicates that SAPRC-07 performs much better with hydrocarbon mixtures containing less aromatic hydrocarbons in highly reactive systems. This problem was not observed in SAPRC-99 for these experiments.
- For all experiments, MCM did not reproduce the observed ozone concentrations accurately, but was closer to observation for the more complex wholly evaporated ULP vapour than for the headspace vapour.

Various updates have been made to the SAPRC-99 mechanism in order to better predict the formation of ozone from various VOCs and to update the peroxy radical chemistry. Significant changes were made to the aromatic mechanism which resulted in modelled improvements for single species-NO_x experiments; however there are still problems in modelling the reactions of species with lower reactivity. Experiments on petroleum/gasoline mixtures indicate that the updated mechanism is less able to predict oxidant formation and concentrations for hydrocarbon mixtures with a significant aromatic concentration. The changes made to the peroxy radical chemistry have not been evaluated in this study, and it is not clear if these changes have impacted on the capability of the model to predict other major pollutants from hydrocarbon mixtures.

1 INTRODUCTION

Air quality model (AQMs) simulations have been extensively used to predict the atmospheric concentrations of photochemical smog oxidants and other pollutants in given airsheds. These simulations can be used to assess the predictive performance of the model and to help define future air quality control strategy options for regulatory purposes. The most used AQMs have an emission inventory component, a meteorological component and a chemical mechanism component.

It is well known that the modelling results for the chemical mechanism component can be affected by uncertainties associated with the mechanisms of various components. More precisely, the existing chemical mechanisms that can be selected to simulate the atmospheric chemistry could lead to large discrepancies in the model results when compared to experimental data (Mallet and Sportisse 2006). Because of the large socio-economic costs associated with the modelling outputs, it is crucial to reduce the risk of errors when using air quality models for policy purposes.

The detailed description of photochemical mechanisms is complicated by the different treatment of the wide range of reactive hydrocarbons VOCs that are emitted by both anthropogenic and biogenic sources. Because of the wide variety of VOCs present in the atmosphere, and the large number of intermediate species involved in the atmospheric chemical reactions, different types of reduced chemical mechanisms have been developed and used to simulate the local and regional air quality of selected airsheds. Given the high uncertainty in various chemical mechanisms, it is unsurprising to find that for selected ozone events for a selected airshed different chemical mechanisms may produce dissimilar results depending on the ambient air mix of pollutants. Differences in the predictions of concentrations of secondary pollutants using different chemical mechanisms have shown the urgent need to develop improved chemical mechanisms that are verified by atmospheric measurements and controlled laboratory experiments.

Photochemical reaction mechanisms suitable for use in air quality simulation models are updated periodically to improve performance or to support wider environmental needs for additional oxidants predictions. One of the major photochemical smog oxidants, ozone, remains a pollutant of particular concern because of its impact on human health and its contribution in the processes and cycles of other secondary pollutants formation.

The Statewide Air Pollution Research Centre (SAPRC) mechanism developed by Carter (2000) is one of the most widely used chemical mechanisms that employs the lumped molecule approach to predict photochemical smog oxidants. The lumped molecule approach represents similar organic species as a single organic compound or as a generalised species. The SAPRC lumped species mechanism can be embedded into AQMs for urban and regional scale modelling.

Recently, Carter (2008) has developed the new updated SAPRC-07 that has been evaluated against ~2400 environmental chamber experiments using over 120 types of VOCs. The mechanism improvements included updated chemical reactions and rate constants, reduced parameterised aromatic mechanisms and different representation for peroxy reactions allowing for Secondary Organic Aerosols (SOA) modelling.

The aim of this work is to assess the performance of SAPRC-07 using the CSIRO smog chamber data. The assessment will report the model performance against data from the smog chamber experiments that were obtained for the studied hydrocarbons/NO_x/air systems. The study did not address issues related to the performance of selected chemical reactions that play key role in the photochemical process. The selected three chemical mechanisms, SAPRC-07, SAPRC-99 and

MCMv3.1 (Bloss et al. 2005), were used and investigated without altering or modifying any chemical reactions or rate constants to adjust the predictions of pollutants. The only exception was that the photolysis rates of key species in MCM were updated to the most recent data available for the appropriate conditions (IUPAC 2006, NASA 2006). Further investigation to address issues or improving these mechanisms may be carried out at a later stage.

2 EXPERIMENTAL

Smog chamber simulations are used to test and develop photochemical smog mechanisms that can be used to predict the formation of photochemical smog oxidants under different conditions. The performance of the chemical mechanisms can be assessed by comparing measured and simulated concentrations over wide ranges of controlled conditions.

To evaluate the performance of the newly developed SAPRC-07 mechanism in simulating oxidant formation, a series of smog chamber experiments using selected key individual VOCs and a complex VOC mix were investigated. These chamber experiments were carried out for ROC/NO_x ratios (for ROC/NO_x expressed as ppbC/ppb) ranging from 28 to 9, with initial NO_x concentrations varied between 25 ppb to 120 ppb.

A series of *m*-xylene, toluene, isoprene and ULP/NO_x/air irradiations were performed in an 18 m³ indoor environmental chamber located at the CSIRO laboratories in Sydney, Australia. The full details concerning the operation of the chamber and the associated instruments have been described previously (Hynes et al., 2005, Angove et al., 2006). To ensure a clean chamber was used for each experiment, the chamber was flushed with highly purified zero air for a minimum of 36 hours including at least 6 hours under irradiation between each experiment.

In preparation for each experiment, the required volume of NO was injected into the chamber as described by Hynes et al. (2005). A known liquid volume of the selected VOC compound was injected into a glass bulb using a SGE micro-syringe and swept into the chamber with N₂ carrier gas. The degradation of the VOC compound was monitored throughout the experiment by Fourier Transform infrared spectrometry (FT-IR) using a Nicolet Magna 550 spectrometer fitted with an MCT detector. The spectra were obtained at a resolution of 1 cm⁻¹ and were an average of 512 scans. Reference spectra for each compound were obtained from the NIST Quantitative Infrared Database (Chu et al. 1999) or from the HANST Infrared Library (Hanst and Hanst 1993). These spectra were individually calibrated in the chamber by injecting known concentrations of the VOC into the chamber and comparing the resulting spectra of known injection volume to the reference spectrum. The difference between the reference spectra and the chamber spectra (assuming complete injection) was found to be negligible for all three hydrocarbons. The NO₂ photolysis rates (J_{NO_2}) for all simulations were determined by NO₂ actinometry as described by Hynes et al. (2005).

For the ULP wholly evaporated experiments, liquid petrol was injected as described above. The headspace samples were prepared by placing 20 mL of ULP in a 200 mL reinforced bottle inserted into a purpose-designed aluminium jacket and equilibrated for 2 hours at 38°C. Sample volumes of 8 mL of the headspace vapour were then injected directly into the chamber using a pre-equilibrated, gas-tight syringe. All experiments used ULP obtained from two batches that was stored at -20 °C between experiments. The first batch was used on all of the wholly evaporated experiments and the second batch was used on the headspace experiments. Initial hydrocarbon concentration were analysed by collecting a small part of the chamber air by canister, and analysing using GC-FID.

Smog chambers used to simulate the photooxidation of VOCs have to be characterised for wall effects, as the heterogeneous chemistry occurring on the walls can modify the radical balance of the gas phase. The CSIRO smog chamber wall effects have been assessed and an auxiliary mechanism has been developed and reported in Hynes et al. (2005), with minor alterations made for this work (see Appendix A).

2.1 Choice of Modelling Scenarios

The current procedures for choosing the modelling scenarios for assessing the SAPRC-07 performance were based primarily on monitoring and comparing the formation and the decay of major chemical species in the smog chamber facility and the use of selected chemical mechanisms to simulate these results. It is well known that when aromatic reactions are incorporated into a selected chemical mechanism, they usually are modified, parameterised and adjusted to fit selected smog chamber observations (Bloss et al. 2005a). This is particularly important when considering urban and industrial atmospheres for which aromatic compounds are a non-negligible component.

For the current assessment it was important to assess the performance of the SAPRC-07 mechanism in reproducing the smog chamber results for experiments that were carried out using aromatic compounds, toluene and *m*-xylene, irradiated in the presence of NO_x. The concentration of aromatics used during the experiments was less than 100 ppb, with less than 80 ppb NO_x. In addition, we have supported the current study by assessing the model performance in terms of reproducing isoprene and unleaded petrol (ULP) because of their importance in most airsheds.

A series of smog chamber experiments were carried out using single species using different ROC/NO_x ratios reflecting the variety of atmospheric conditions. Table 1 shows the list of the smog chamber experiment initial conditions that were used to simulate photochemical oxidants and other species using MCMv3.1 (from now MCM), SAPRC-99 and SAPRC-07.

All experiments were conducted for 6 hours, except for two isoprene experiments (experiment 303 for 10.5 hours and experiment 304 for 14 hours). For all non-ULP injections, initial HONO was specified using equation (1), as outlined in Appendix A.

$$[\text{HONO}]_0 = 0.11 + (3.3 \times 10^{-3}) [\text{NO}_x]_0 \text{ ppb} \quad (1)$$

For the ULP experiments, a HONO generator (Febo et al. 1995) was turned on 10 minutes before lights were turned on, and this injected HONO into the chamber continuously for the entirety of the experiment. For these experiments, all having similar initial NO_x concentrations, the initial HONO was set at 0.6 ppb. The HONO generation rate was determined to be about 1.5 ± 0.5 ppb hour⁻¹.

As the formation of photochemical smog oxidants is mainly driven by reaction of organic species with the OH radical, as well as secondary reactions involving HO₂ and RO₂ radicals, it is important to determine how the production rates of these radicals predicted by each model compared with other model predictions. In addition, if the model is intended to be used for predicting the potential formation of SOA, it is critical for the mechanism to predict accurately the amount of the OH radical during the experiment. With the absence of an instrument to measure these radicals at the CSIRO chamber, in the current assessment we have used OH and HO₂ values predicted by the selected mechanisms to generate an assessment of OH accuracy.

Table 1: List of smog chamber experiments modelled

Exp.	Species / J_{NO₂}	HC / ppb	NO_x / ppb	ROC/NO_x (ppbC / ppb)
303	isoprene / 0.41	350	114	15.4
304	isoprene / 0.41	88	38	11.6
447	isoprene / 0.39	190	75	12.7
448	isoprene / 0.39	360	75	24.0
412	toluene / 0.43	89	33	18.9
429	toluene / 0.43	88	73	8.4
431	toluene / 0.43	92	49	13.1
416	<i>m</i> -xylene / 0.43	88	70	10.1
418	<i>m</i> -xylene / 0.43	64	70	7.3
419	<i>m</i> -xylene / 0.43	37	71	4.2
421	<i>m</i> -xylene / 0.43	64	47	10.9
423	<i>m</i> -xylene / 0.43	90	49	14.7
424	<i>m</i> -xylene / 0.43	37	50	5.9
425	<i>m</i> -xylene / 0.43	64	35	14.6
426	<i>m</i> -xylene / 0.43	37	35	8.5
428	<i>m</i> -xylene / 0.43	92	36	20.4
362	ULP injection / 0.45	1401.1 (ppbC)	135	10.4
363	ULP injection / 0.45	1419.7 (ppbC)	137	10.4
369	ULP headspace / 0.44	1148.5 (ppbC)	135	8.5
403	ULP headspace / 0.46	1044.1 (ppbC)	136	7.7

All experiments were performed at low humidity (2-5% relative humidity) except for the ULP experiments which were performed at approximately 50% relative humidity. The temperature of each experiment varied slightly, but typically started at between 293-298 K before increasing over the first hour to 302-309 K where it remained constant to the end of the experiment.

2.2 *m*-Xylene

Nine *m*-xylene smog chamber experiments were modelled using SAPRC-07, SAPRC-99 and MCMv3.1. These experiments were carried out for ROC/NO_x (expressed in this report as ppbC/ppb) ratios varying between 7.3 and 20.4. The nine experiments form a 3 × 3 matrix, with initial hydrocarbon measurements of approximately 90, 64 and 38 ppb, and initial NO_x measurements of approximately 34, 50 and 68 ppb. For all these experiments, J_{NO₂} was measured at 0.43 min⁻¹. The initial conditions for the smog chamber experiments are given in Table 1.

The smog chamber data and the simulated ozone produced for the experiments with initial hydrocarbon concentration of about 64 ppb for the various mechanisms are illustrated in Figures 1, 2 and 3. These results show that the selected two SAPRC chemical mechanisms have successfully reproduced the smog chamber data for ozone formation for the range of ROC/NO_x ratios of 14.6, 10.9 and 7.3.

During the first hour of the simulation, both SAPRC mechanisms have produced higher ozone concentrations than observed, which was associated with a fast rate of NO oxidation and comparable rates of *m*-xylene oxidation. This was particularly true for high ROC/NO_x experiments. For the same period, SAPRC mechanisms have produced the highest OH concentrations, with SAPRC-07 having a higher OH concentration than SAPRC-99, but both have equivalent ozone formation. After the first hour of the experiment, the ozone predicted by SAPRC-07 and 99 compared very well (within 15%) to observation, while the amount of *m*-xylene present was somewhat higher than observed.

In general, the ozone concentrations predicted by the MCM mechanism compared less favourably to observations than the SAPRC ozone predictions. The rate of NO oxidation predicted by MCM compare reasonably well with observation for the initial stages, but during the most active oxidation period the concentration of OH present is not sufficient for the model to match NO₂ or ozone formation. The final ozone amount predicted by MCM after the oxidation period also appears to have higher modelled error than that predicted by SAPRC.

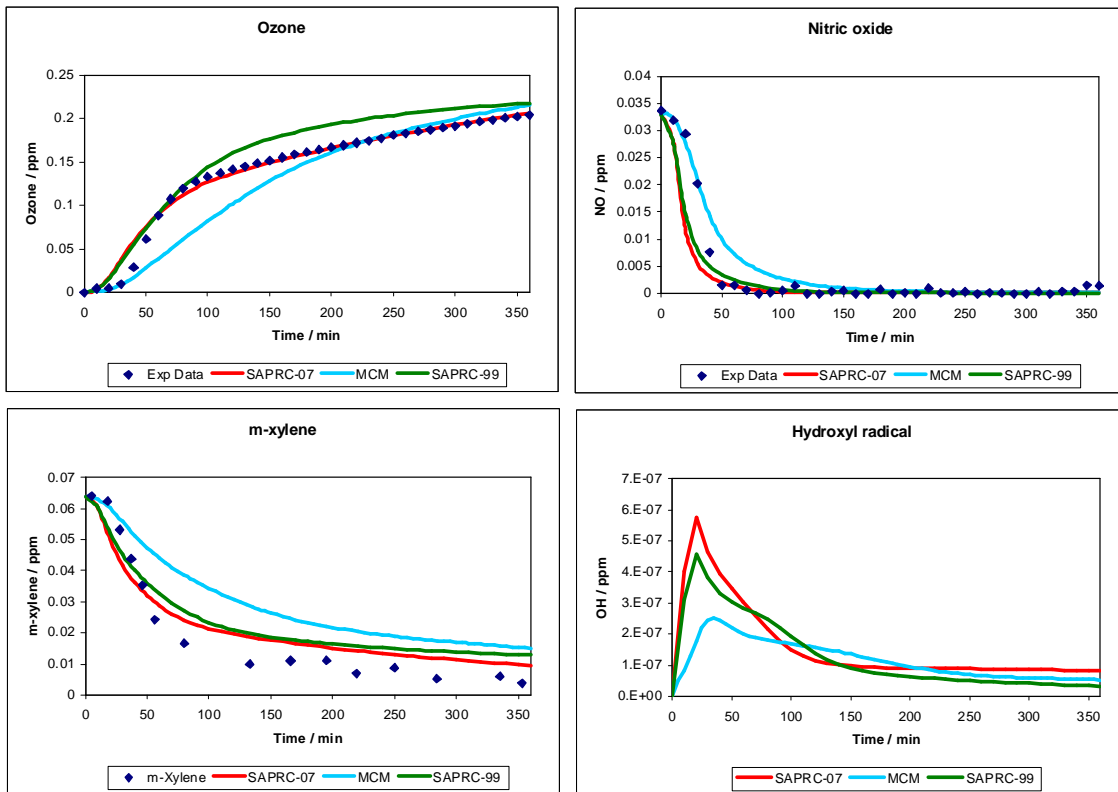


Figure 1: Modelled results for experiment 425 (*m*-xylene: 64 ppb; NO_x: 35 ppb; ROC/NO_x: 14.6)

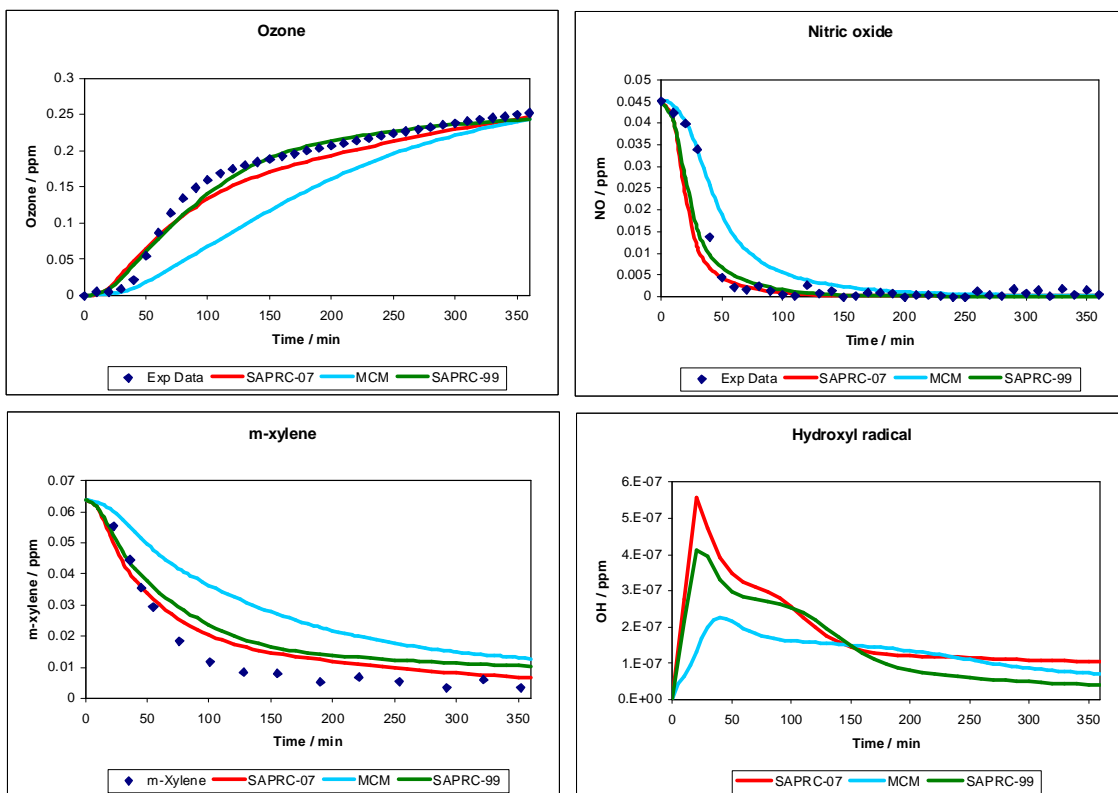


Figure 2: Modelled results for experiment 421 (*m*-xylene: 64 ppb; NO_x: 47 ppb; ROC/NO_x: 10.9)

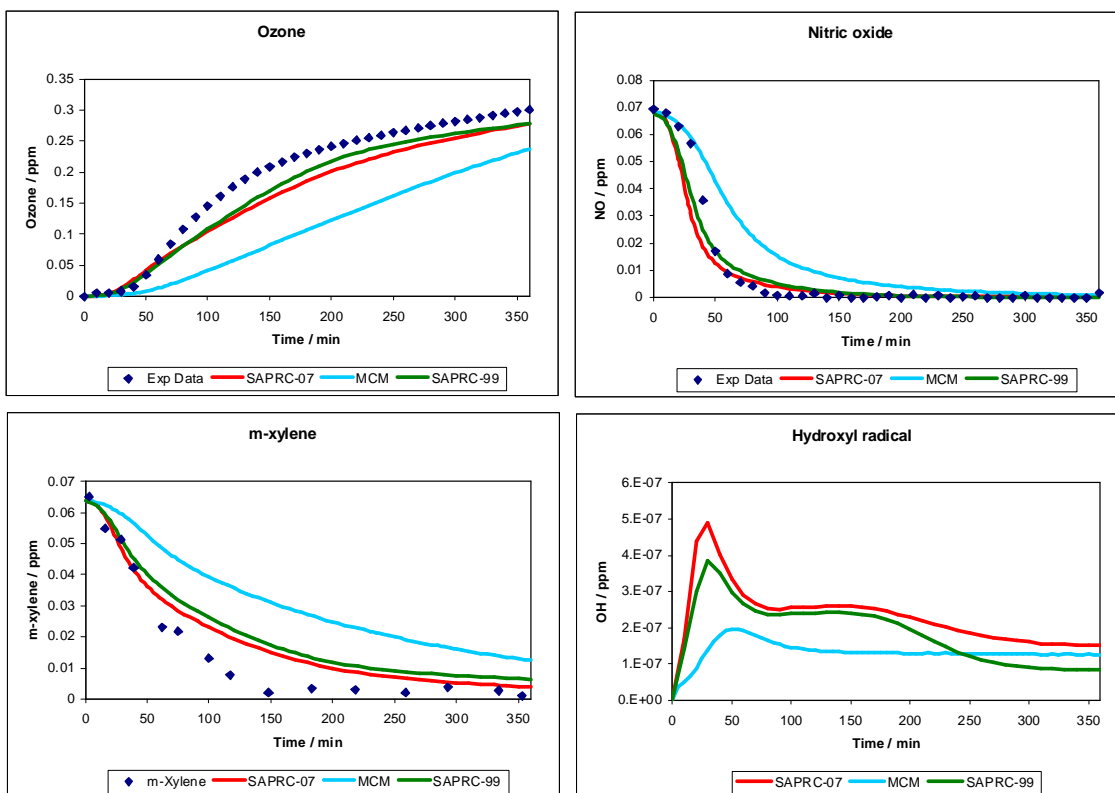


Figure 3: Modelled results for experiment 418 (*m*-xylene: 64 ppb; NO_x: 70 ppb; ROC/NO_x: 7.3)

The modelled results for experiments with an initial *m*-xylene concentration of 90 ppb are shown in Figures 4, 5 and 6. Both SAPRC mechanisms predicted higher ozone concentrations during the first hour of the experiment, than were observed. This is characterised by early onset of ozone formation, fast NO oxidation, and initially fast *m*-xylene degradation which matches observation after the first 30 minutes. After the first hour of the experiment, both mechanisms have predicted ozone profiles that are in good agreement with observations, with the degradation of *m*-xylene again overestimated by SAPRC. In general, SAPRC-07 predictions for ozone concentrations were much slightly to observations than SAPRC-99 predictions.

The MCM mechanism again predicted a slower ozone formation rate than was observed experimentally, and this is because of insufficient OH during the first 90 minutes of the experiment. This is likely due to not enough peroxy radicals (likely HO₂) being formed from the reaction of the ring-opening aromatic product, which propagates the photooxidation reactions by rapidly replenishing OH radicals in the presence of NO_x. This is not a problem observed in the SAPRC mechanisms.

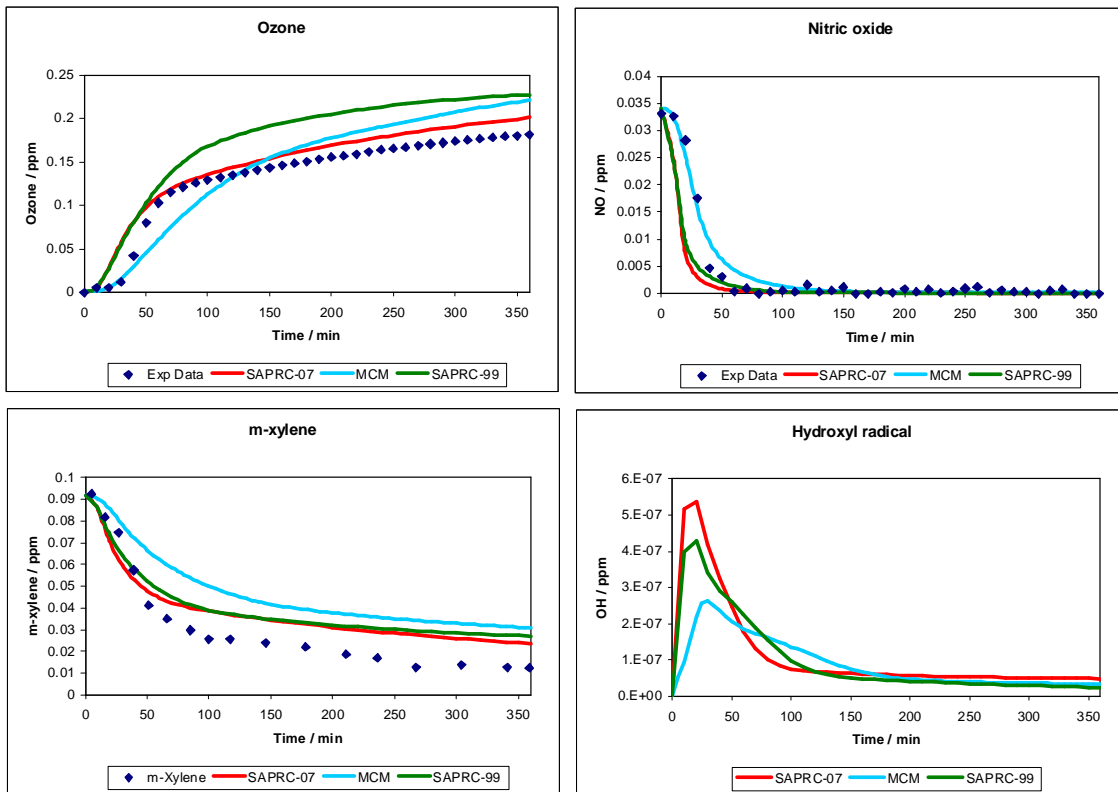


Figure 4: Modelled results for experiment 428 (*m*-xylene: 92 ppb; NO_x: 36 ppb; ROC/NO_x: 20.4)

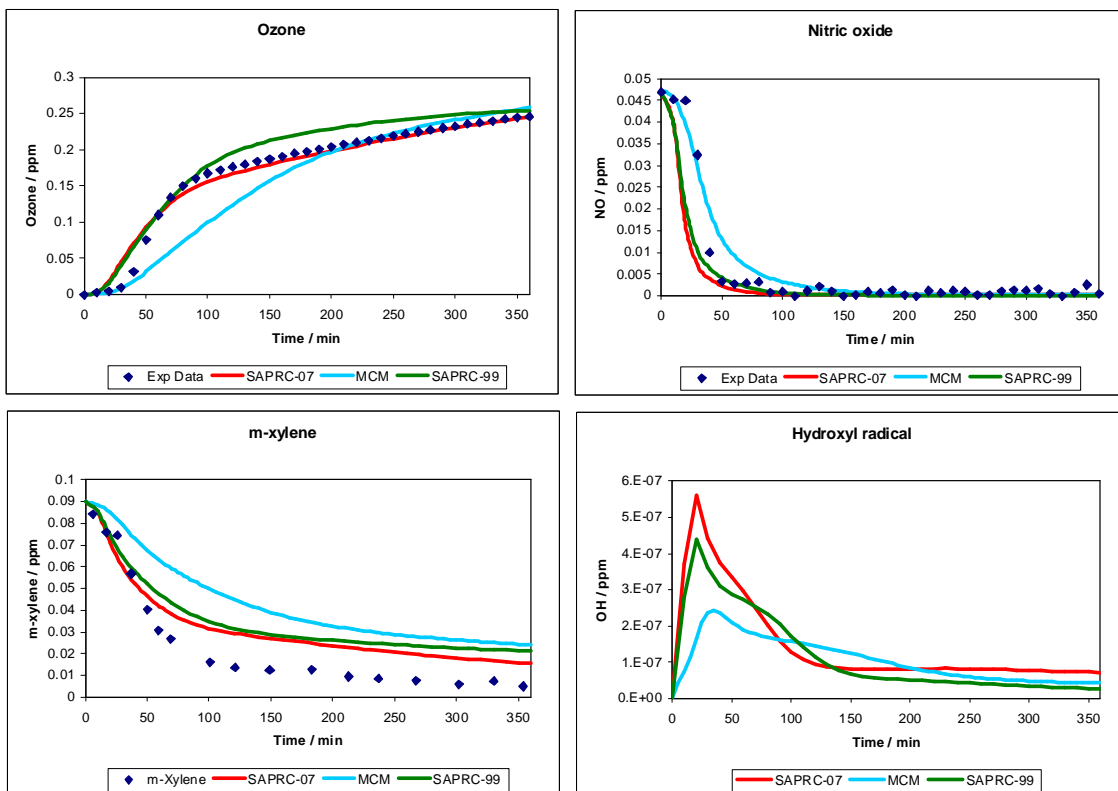


Figure 5: Modelled results for experiment 423 (*m*-xylene: 90 ppb; NO_x: 49 ppb; ROC/NO_x: 14.7)

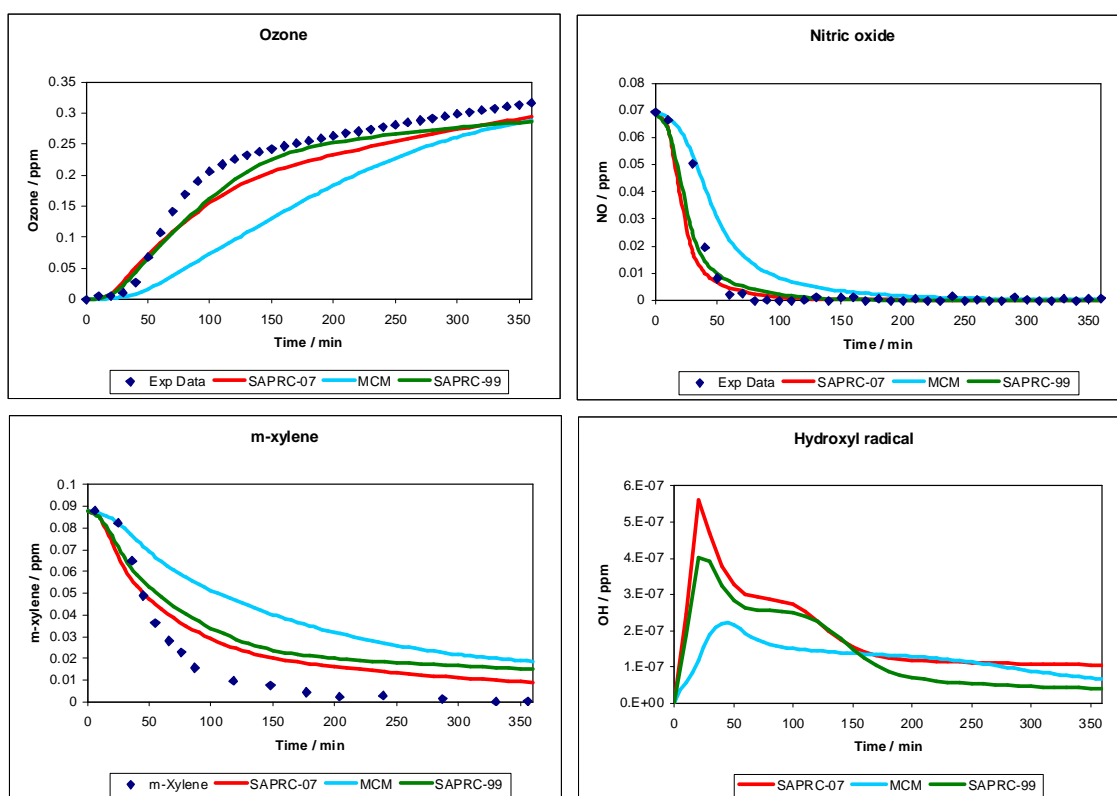


Figure 6: Modelled results for experiment 416 (*m*-xylene: 88 ppb; NO_x: 70 ppb; ROC/NO_x: 10.1)

One way to describe the performance of a model in predicting the formation of ozone under both hydrocarbon and NO_x-limited conditions is to use the term $\Delta(O_3\text{-}NO)$ (Carter 2000), defined in equation (2).

$$\Delta(O_3\text{-}NO) = ([O_3]_t - [O_3]_0) - ([NO]_t - [NO]_0) \quad (2)$$

A summary of the observed and modelled $\Delta(O_3\text{-}NO)$ is given in Table 2. The table is ordered according to initial NO_x (the first three rows are $[NO_x]_0 = 33$ ppb, second set of three rows are $[NO_x]_0 = 50$ ppb and the last set of three rows are $[NO_x]_0 = 68$ ppb. For the low-NO_x experiments, SAPRC-07 performed better than SAPRC-99 at predicting the final ozone amount, although they were mostly overestimated but still within 10% of the observed values. For the mid-NO_x and high-NO_x experiments, both models reproduced $\Delta(O_3\text{-}NO)$ to within 8% with the exception of the low hydrocarbon experiments (424 and 419) which were still forming significant ozone after 6 hours.

Table 2: Maximum ozone concentrations for the *m*-xylene selected smog chamber experiments. All values are given at 6 hours (experiment completion)

Exp	ROC / NO _x (ppbC / ppb)	Δ(O ₃ -NO) (ppb)	SAPRC-07 Δ(O ₃ -NO) (ppb)	SAPRC-99 Δ(O ₃ -NO) (ppb)	Average Δ(O ₃ -NO) Model Error (SAPRC -07 / -99) (%)
428	20.4	215	235	261	9.3 / 21.4
425	14.6	236	239	250	1.3 / 5.9
426	8.5	234	229	235	-2.1 / 0.4
423	14.7	292	292	301	0 / 3.1
421	10.9	297	291	289	-2 / -2.7
424	5.9	275	247	263	-10.2 / -4.4
416	10.1	385	362	355	-6 / -7.8
418	7.3	368	346	346	-6 / -6
419	4.2	293	223	253	-23.9 / -13.7

The difference between SAPRC-07 and SAPRC-99 can best be shown by monitoring the model bias for Δ(O₃-NO) over the course of the experiment (Figure 7). For both models, the legend showing the experiment number has been arranged in decreasing order for the final error, with the experiment number labelled (followed by the ROC/NO_x ratio in brackets). For both models, there appears to be ROC/NO_x dependence, with higher ratio experiments invariably having positive error, and smaller ratio experiments having negative error. The low ratio experiments (419 and 424) show negative error because unlike the high ratio experiments the reactivity in the initial stages of oxidation is underestimated.

While the final Δ(O₃-NO) values are similar for SAPRC-07 and SAPRC-99, it can be seen at around 100-150 minutes into the experiments SAPRC-07 performs better at predicting oxidant yield. For most of the experiments thereafter the model error does not change much, while it varies more for SAPRC-99, indicating better rate of oxidation prediction for SAPRC-07. Another difference is that once a reasonably steady state has been established for the Δ(O₃-NO) values, the SAPRC-07 ones increase slightly compared to experimental, whereas SAPRC-99 decreases at a larger rate. This is most likely due to changes in the inorganic or basic organic mechanism, which leads to a higher OH concentration for the NO_x limited regime at the end of the experiment for SAPRC-07 (see Figures 1-6).

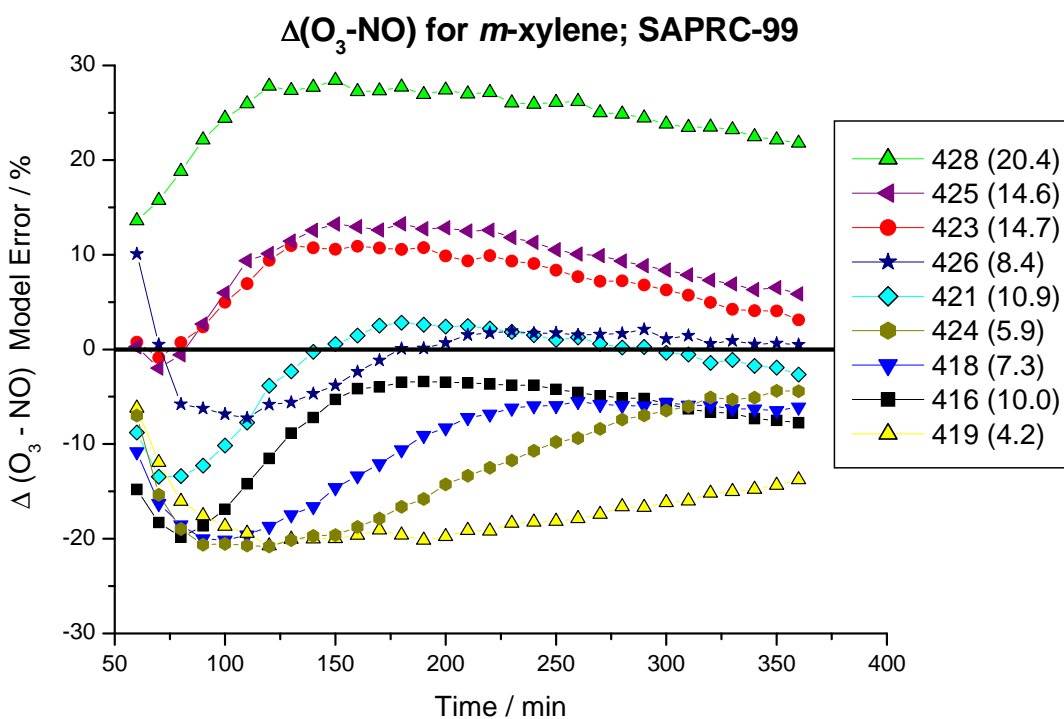
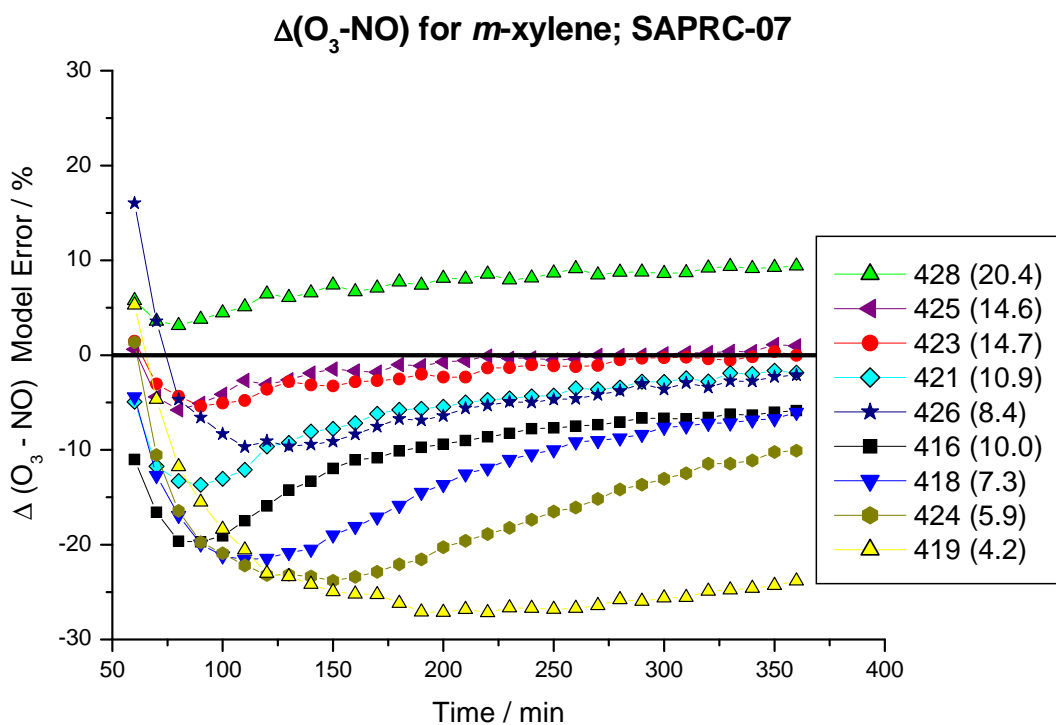


Figure 7: Modelled errors for $\Delta(O_3-NO)$ for (a) SAPRC-07 and (b) SAPRC-99 for *m*-xylene experiments

Shown in Appendix B are extended mechanism evaluations for two *m*-xylene experiments (416 and 428). Where possible, comparison of modelled species with experimental values determined using FT-IR has been provided, otherwise direct comparison between the models is provided. The final ozone predicted for experiment 428 is higher than observed, and for experiment 416 it is lower than observed, and this is consistent across all three models used. In addition to comments earlier on these experiments regarding OH concentration, the concentration of HO₂ is predicted similarly in the models, but slightly higher in the latest update to SAPRC, which is consistent with the small increase seen in OH radical concentration. The term NO_y-NO describes the difference between total NO_x and NO measured by a chemiluminescent analyser, and as such uses the term NO_xNA-NO from SAPRC (which includes organic nitrates, PANs and total inorganic NO_y, not including NO). For the MCM shown, the NO_y term includes all organic nitrogen species not including organic nitrates (but including organic peroxy nitrates). In each aromatic experiment chemiluminescent detectable NO_y is lost, and this is not accounted for in the mechanism, and to the best of the authors' knowledge, the pathway leading to loss of observable NO_y in these experiments has not been fully explained.

The models generally predict major oxidants well. Formaldehyde is higher in SAPRC-07 and closer to experimental values, particularly for the low NO_x experiment. However for experiment 416, the formaldehyde is 60% higher in SAPRC-07 than observed. None of the models however predict the formation of carbon monoxide adequately, which has direct implication on the OH concentration predicted. This excess CO probably arises from the hydrocarbon itself, from the photolysis and reaction of some of its secondary products. The formation of formic acid is not predicted in any of the mechanisms, but is likely to result as a consequence of the photolysis and reactions of aldehydes, in particular species like glyoxal (Tadić et al. 2006). Whilst formic acid will form from the oxidation of formaldehyde, the concentrations of formic acid as reported in the isoprene work (see Section 3.4) are equivalent to those of the aromatic experiments, despite the fact that formaldehyde is in considerably higher concentration in the isoprene experiments. This indicates the formic acid likely forms as a result of products formed in higher concentration in the aromatic experiments, such as dicarbonyl species.

The formation of nitrogen-containing species is reasonably well predicted by both models. Nitric acid formation is predicted better for SAPRC-99, and this could be because of nitrogen appearing to react with organic molecules more favourably in SAPRC-07, thereby depleting the amount of inorganic nitrogen available. Peroxy acetyl nitrate (PAN) is estimated well by both models, however in the low NO_x experiment the amount formed by 80 minutes is almost double that observed in both SAPRC models. The measurement of PAN is problematic as it may include other PAN species, which can share similar absorbances, but will be lower in concentration. The infrared band used to measure PAN was that centred at 1163 cm⁻¹ using spectra from Allen et al. (2005). The characteristics of the two experiments shown here are characteristic of all tested *m*-xylene experiments for which measurements were available.

2.3 Toluene

Three toluene smog chamber experiments were carried out to assess the SAPRC and MCM mechanisms ability to reproduce the observed ozone and other major photochemical smog species. All three toluene experiments modelled have approximately the same initial hydrocarbon concentration of 88 ppb, 89 ppb and 92 ppb. The NO_x concentrations injected in the chamber were 73 ppb, 49 ppb and 33 ppb producing ROC/NO_x ratios of around 8.4, 18.9 and 13.1 respectively (Figures 8, 9 and 10). These experiments were carried out at J_{NO₂} of 0.43 min⁻¹.

The ozone levels predicted by all the selected models were lower than observations; however, the ozone concentrations predicted by SAPRC-07 mechanism were closer to observed concentrations than the other two mechanisms. The maximum OH concentration of around 3.8×10^{-7} ppm was predicted by SAPRC-07 for ROC/NO_x = 18.9 after around 50 minutes from the start of the experiment. The low rate of ozone formation and toluene degradation when compared to observations was matched by the low rate of NO oxidation from each simulation. The problems in predicting the rate of oxidation for all toluene experiments could be indicative of problems with the mechanism of less reactive mono-substituted aromatic hydrocarbons like toluene when compared to much more reactive di- and tri-substituted aromatic hydrocarbons such as *m*-xylene or mesitylene. This simulated reactivity underprediction is surprising given that initial NO oxidation and O₃ formation was overestimated for toluene-NO_x blacklight experiments and outdoor experiments in the UNC chamber and reasonable estimates using SAPRC-07 (Carter 2008 pp. 83). As with *m*-xylene, the MCM model predicts slower ozone formation when compared with the SAPRC models.

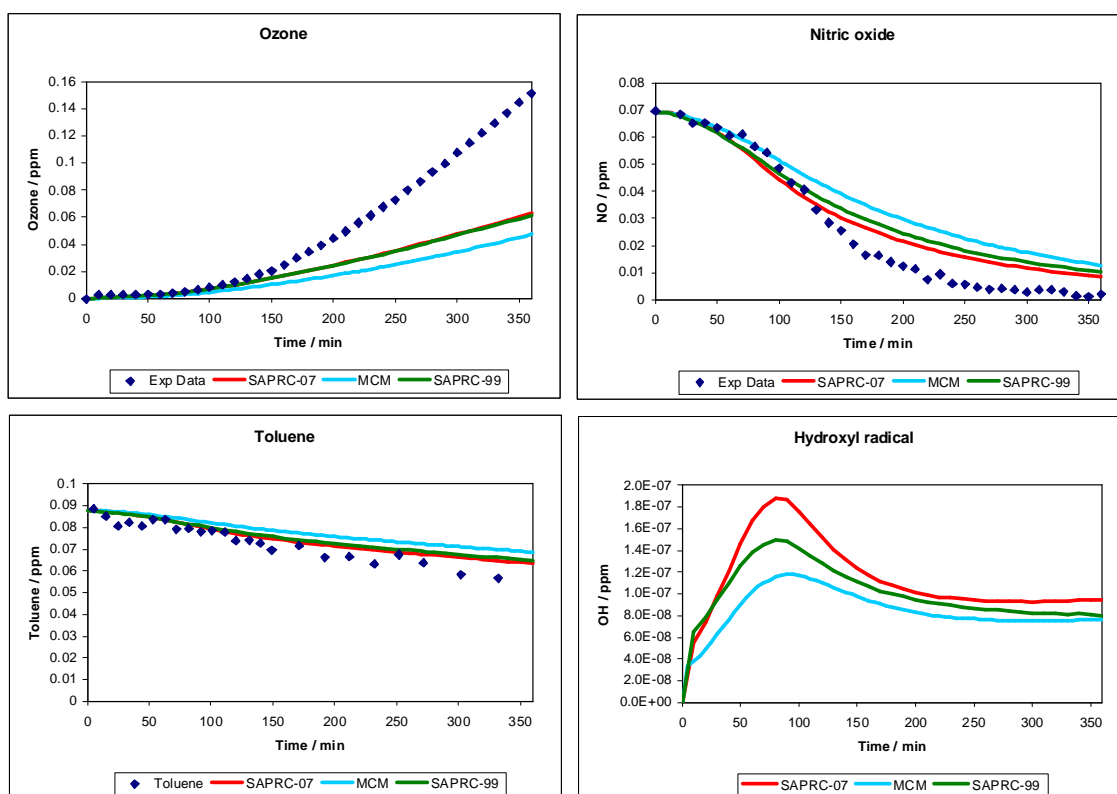


Figure 8: Modelled results for experiment 429 (toluene: 88 ppb; NO_x: 73 ppb; ROC/NO_x: 18.9)

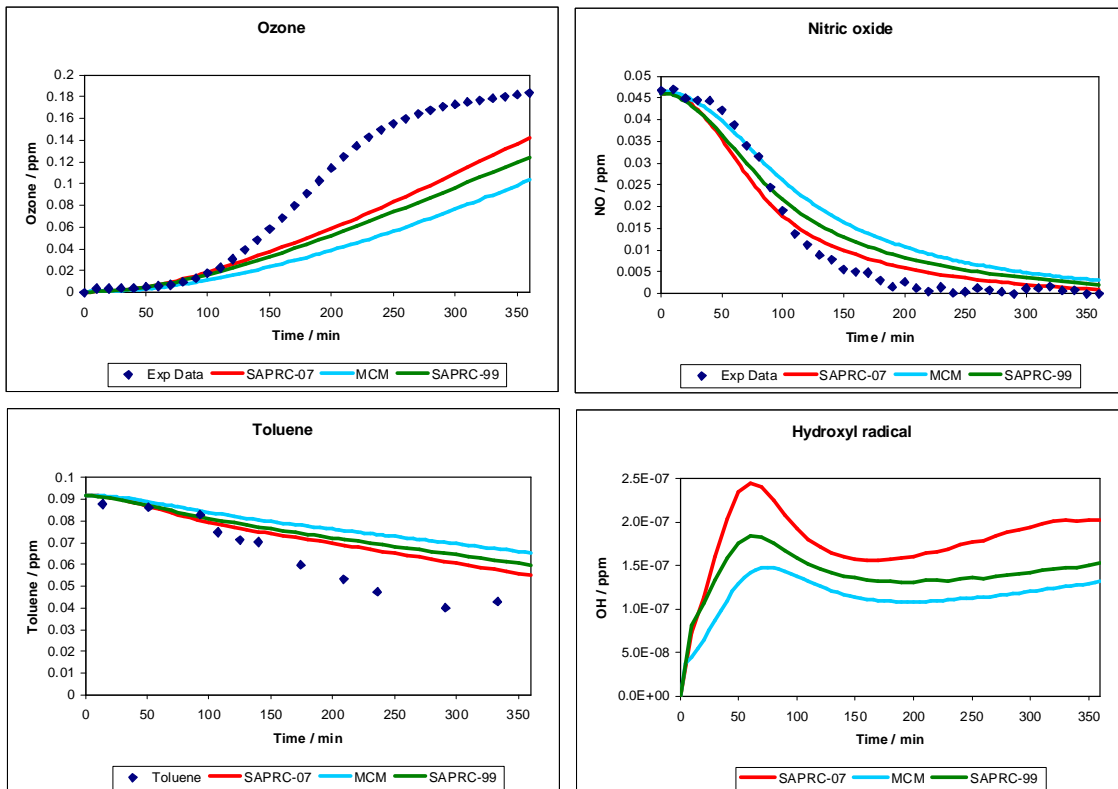


Figure 9: Modelled results for experiment 431 (toluene: 92 ppb; NO_x: 49 ppb; ROC/NO_x: 13.1)

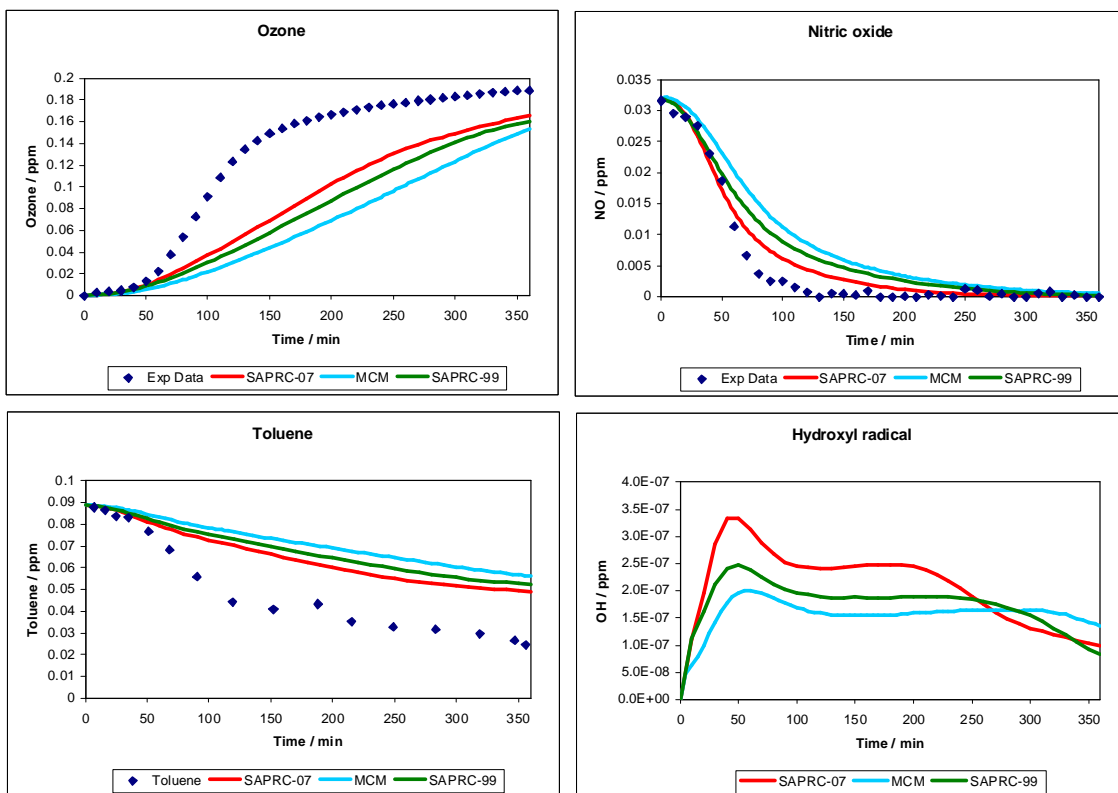


Figure 10: Modelled results for experiment 412 (toluene: 89 ppb; NO_x: 33 ppb; ROC/NO_x: 18.9)

The slow rate of oxidation observed in simulations of toluene-NO_x experiments can be explained by observing the concentration of OH radical predicted for these experiments, which is the primary reactant of aromatic hydrocarbons. As a comparison, two experiments with approximately equivalent initial VOC and NO_x for toluene (412) and *m*-xylene (428) are shown in Figure 11 for predicted and observed ozone and predicted OH concentrations. As expected, the reaction of *m*-xylene is quicker than toluene, with a short oxidation period in which most of the ozone is formed occurring between 20-60 minutes. Toluene has a longer oxidation period that occurs between 40-150 minutes. SAPRC-07 predicts the initial oxidation period, characterised by a large increase in OH radical concentration, well for *m*-xylene. It does not however predict this same period well for the toluene experiment, with only a small increase in OH concentration observed at around 50 minutes.

It is clear that for the toluene mechanism to predict oxidant products accurately, a peak of OH similar to that observed for *m*-xylene experiments needs to occur over a slightly longer period for the toluene experiment. Given the complex interaction of OH, HO₂, organics and NO_x, it is difficult to ascertain which reactions need to be altered to produce a higher OH radical concentration during this oxidation event. Given that the largest OH producing reaction in the chamber mechanism is likely to be the reaction of NO with HO₂, this may indicate that insufficient amounts of HO₂ are being formed in the mechanism for the reaction of toluene and the OH radical.

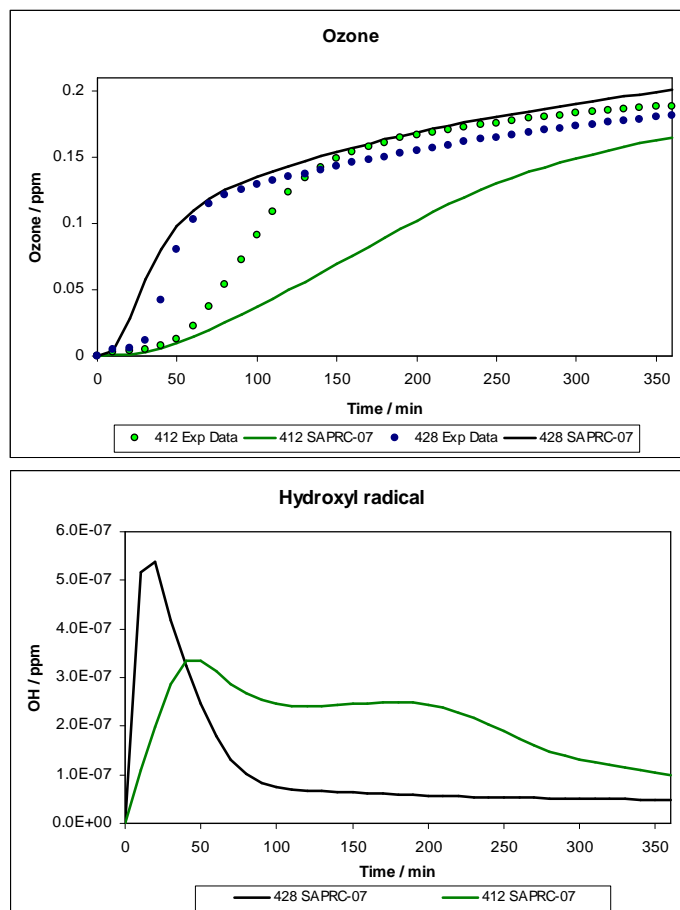


Figure 11: Comparison of (a) ozone and (b) OH concentration for exp 412 (toluene 89 ppb, NO_x 35 ppb) and exp 428 (*m*-xylene 92 ppb, NO_x 36 ppb)

2.4 Isoprene

Four smog chamber experiments containing isoprene/ NO_x were performed and simulated using SAPRC-07/99 and MCM. All experiments were carried out using similar light intensity, with a NO_2 photolysis rate J_{NO_2} of 0.41 min^{-1} or 0.39 min^{-1} . The initial isoprene concentrations ranged from 88 to 360 ppb, with initial NO_x between 38 and 114 ppb. Figures 13 through 16 illustrate the comparison of experimental and predicted concentration-time profiles for isoprene, NO , O_3 and OH .

The modelling results of the irradiation of the isoprene/ NO_x mixtures showed that the selected chemical mechanisms have performed reasonably well in predicting the initial ozone formation, however all models underestimated the final ozone amount by between 20-30% (including CB05 model results for these experiments not shown here). Both versions of SAPRC predicted isoprene degradation and NO oxidation accurately, with the differences between the models in onset of oxidation attributable largely to the reduction in HONO photolysis rate to OH and removal of HONO photolysis to form HO_2 in the updated SAPRC mechanism. No noticeable difference was observed between MCM and SAPRC, despite the $\text{O}(^3\text{P})$ chemistry not being included in the MCM mechanism (Pinho et al. (2005)).

All selected models predicted the onset of the NO -limited conditions but failed to reproduce the continual observed ozone increase at the point of onset of the NO limited regime. Given the formation of ozone is dependent on the available gas-phase NO_y , it is likely that the underestimation of ozone during the period when NO first becomes limited is related to available NO_y at that point in time. The predictions of NO_y species for SAPRC-07 are shown in Figure 12, for the concentration of inorganic NO_y – NO , PAN species and organic nitrates (RNO_3), with the highlighted period between 150 and 210 minutes indicating the region where the modelled and experiment ozone results differ in formation rates. It is difficult to determine which reaction is responsible for this ozone discrepancy, but as ozone is formed primarily from the photolysis of NO_2 , it would appear that increasing the concentration of NO_2 in this period (or effectively increase $\text{O}(^3\text{P})$) would have the direct effect of increasing ozone. This may be accomplished by altering the rate of nitrate or PAN formation, or increasing the thermal decomposition of these species, thereby increasing the available NO_2 .

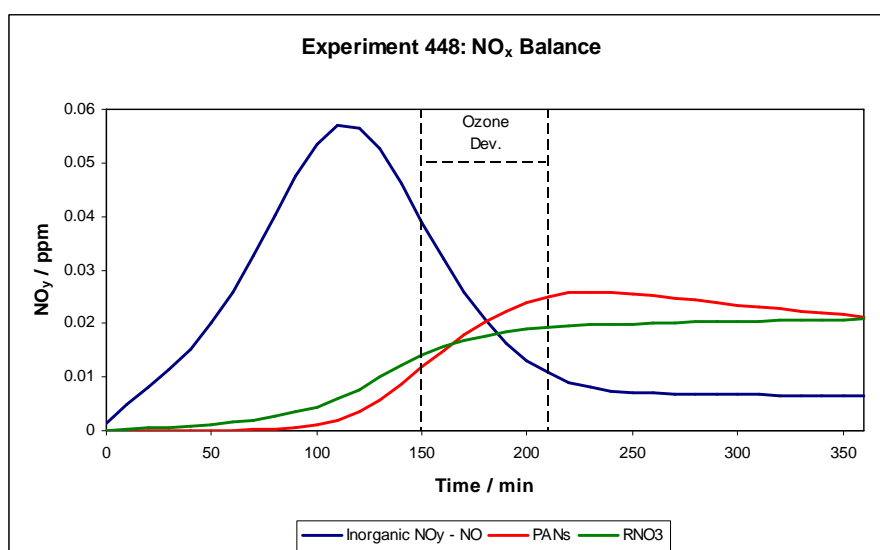


Figure 12: SAPRC-07 NO_y species for experiment 448 (isoprene: 360 ppb; NO_x : 75 ppb).
Inorganic NO_y - $\text{NO} = \text{NO}_2 + \text{NO}_3 + \text{HONO} + \text{HNO}_3 + \text{HNO}_4 + (2 \times \text{N}_2\text{O}_5)$

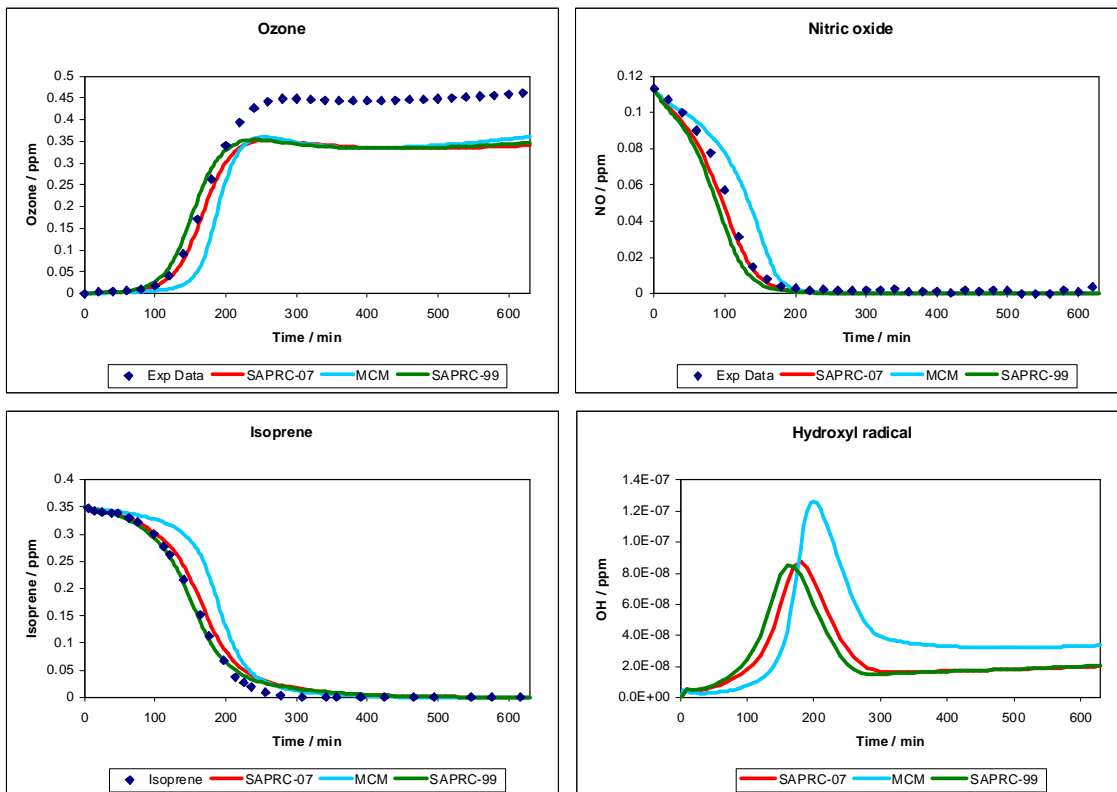


Figure 13: Modelled results for experiment 303 (isoprene: 350 ppb; NO_x: 114 ppb; ROC/NO_x: 15.4)

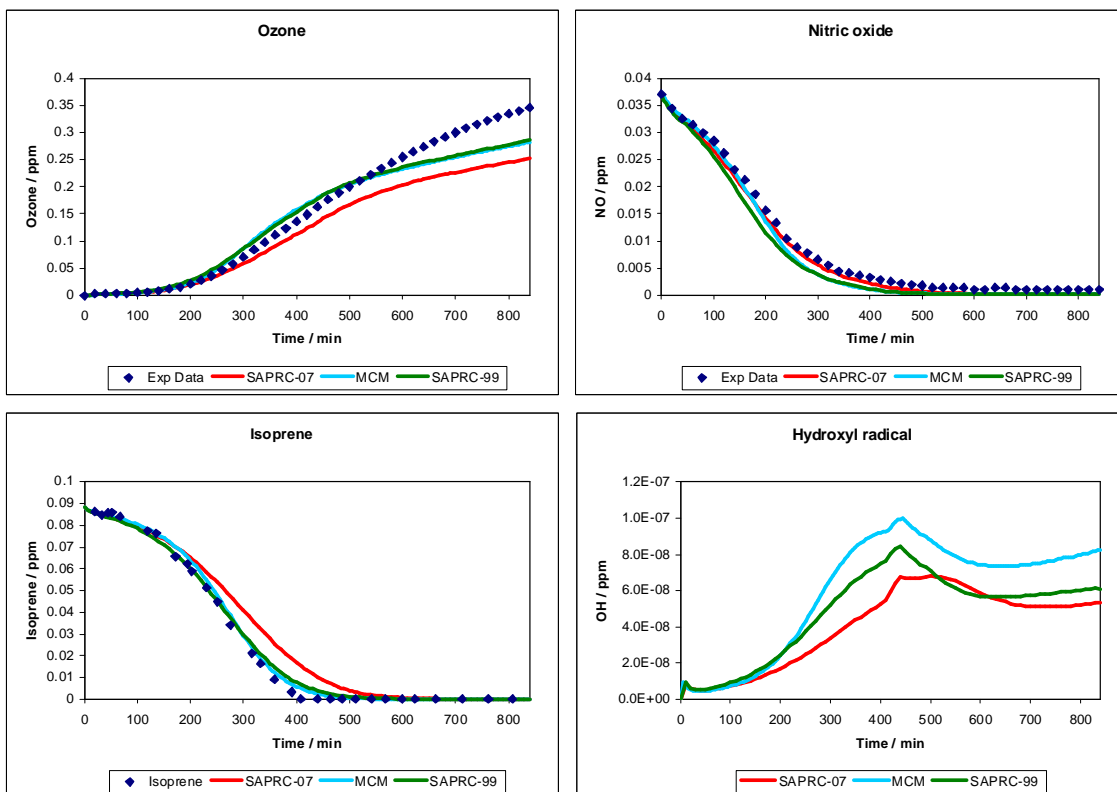


Figure 14: Modelled results for experiment 304 (isoprene: 88 ppb; NO_x: 38 ppb; ROC/NO_x: 11.6)

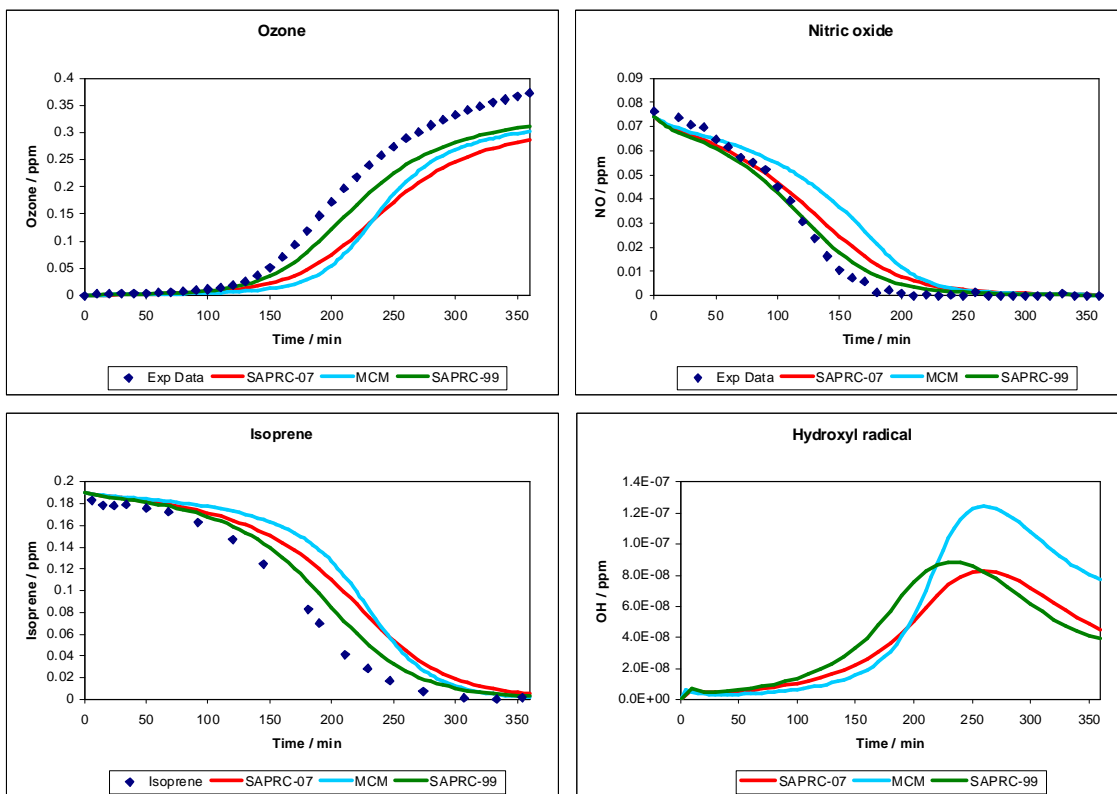


Figure 15: Modelled results for experiment 447 (isoprene: 190 ppb; NO_x : 75 ppb; ROC/NO_x : 12.7)

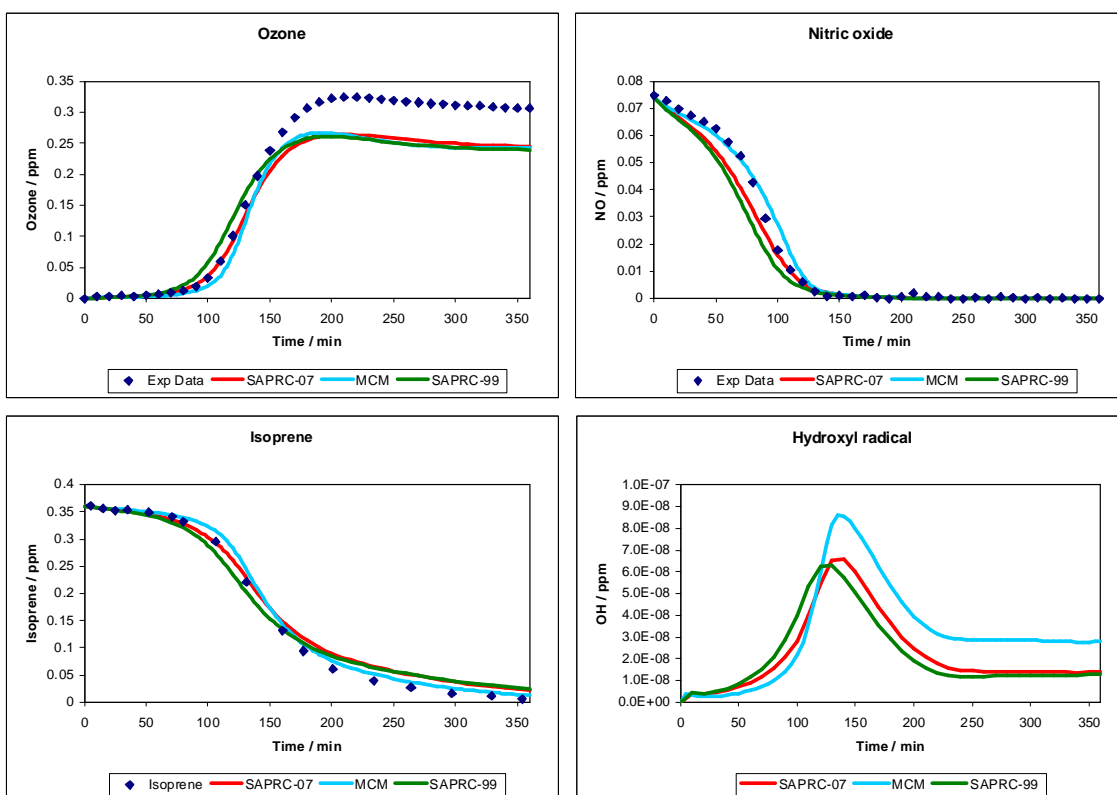


Figure 16: Modelled results for experiment 448 (isoprene: 360 ppb; NO_x : 75 ppb; ROC/NO_x : 24.0)

The formation of other species from isoprene photooxidation was monitored and can be seen for two of the experiments (304 and 448) in Appendix C. Both experiments predict ozone formation well until the NO-limited region as shown above. Similarly to the aromatic experiment, chemiluminescent NO_y loss is observed during the oxidation period, and it is likely to be the reaction of NO_x with organic species that give products with limited or no response on the detector, as is shown by the dotted red line for SAPRC-07 which does not include nitrate (but does include PAN species). The MCM result for NO_y-NO does not include organic nitrates.

The formation of other species is also modelled well for all models. Formaldehyde is predicted reasonably well for all models, however it is underpredicted for SAPRC and is lower in the updated version. There does not appear to be any major difference between the predictions of MVK and methacrolein between SAPRC-07 and SAPRC-99, however experimental results were not able to be obtained for these two species. Formic acid is largely overestimated by SAPRC-99 but is underpredicted for SAPRC-07 and MCM, whereas carbon monoxide is underpredicted by both SAPRC models and overpredicted slightly for MCM. The analysis of PAN is problematic (see Section 3.2) but it does appear to be better predicted using SAPRC rather than MCM, with a slight decrease observed in the updated mechanism.

2.5 ULP Experiments

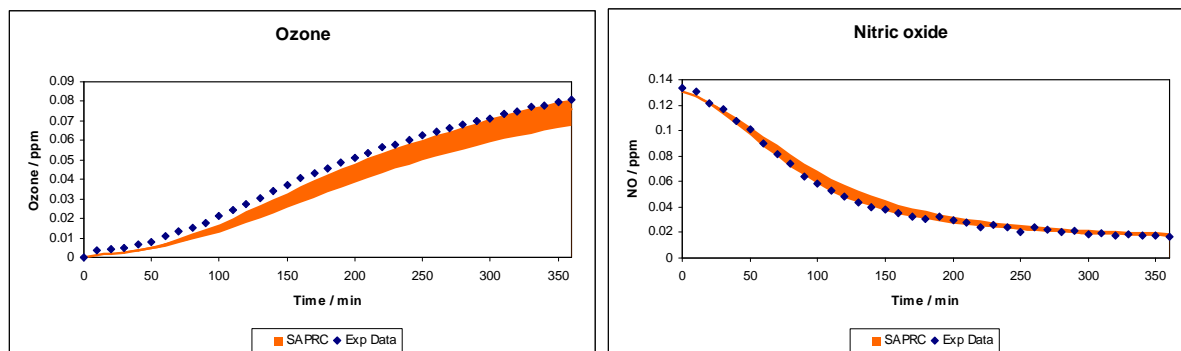
Two experiments were performed with wholly evaporated ULP in the presence of NO_x (experiments 362 & 363). Two further experiments (experiments 369 and 403) were performed with partially evaporated ULP (headspace vapour) in the presence of NO_x. All experiments were performed at approximately 50% relative humidity with a HONO generator used constantly throughout the experiment. The approximate VOC compositions as determined by GC-FID are shown in Table 3.

Table 3: Hydrocarbon composition for the selected ULP experiments.
All measurements are in ppb (ppbC).

Experiment	Total HC	Alkane	Alkene	Aromatic	Dienes	Other*
362	216.2 (1401.1)	116.7 (691.1)	31.1 (166.9)	67.4 (539.3)	0.1 (0.7)	0.9 (3.2)
363	219.3 (1419.7)	118.5 (701.2)	32.1 (172.2)	67.9 (543.4)	0.3 (1.3)	0.5 (1.3)
369	237.1 (1148.5)	174.3 (857.0)	55.9 (242.3)	6.2 (45.7)	0.6 (2.9)	0.1 (0.4)
403	213.0 (1044.1)	158.9 (782.6)	46.8 (214.5)	5.3 (37.6)	0.8 (3.7)	1.1 (5.7)

* Includes unidentified species and acetylene.

Unlike the other experiments evaluated in this study, the ULP experiments were performed with HONO added constantly. The generation rate was determined to be between 1 ppb hour⁻¹ and 2 ppb hour⁻¹. Changing the HONO generation rate does have a moderate impact on predicted ozone formation in the model as can be seen in Figure 17 for experiment 369. In this case the lower bound uses a HONO formation of 1 ppb hour⁻¹ and the upper bound a HONO formation rate of 2 ppb hour⁻¹. The difference observed for nitric oxide oxidation rate was not large.



**Figure 17: SAPRC-07 ozone and nitric oxide profiles for experiment 369
(lower bound: HONO gen = 1.0 ppb hr⁻¹; upper bound: HONO gen = 2.0 ppb hr⁻¹)**

The difference between the lower and upper bound amounts to a difference of 20% in the final ozone amount, and this is similar to the difference observed in ozone for different HONO generation rates modelled using wholly evaporated ULP experiments. As HONO cannot be measured accurately at low concentrations in the CSIRO chamber, this uncertainty needs to be accounted for when analysing these results.

For experiments with a wide variety of hydrocarbons present, assumptions need to be made to simplify the reactivity of the hydrocarbons for effectively modelling. For SAPRC-99 and SAPRC-07, species were included by their detailed model species (DMS) name if it had been characterised, otherwise the species was included in a lumped DMS analogue (e.g. C10-BEN2 for C10 di-substituted benzenes like *p*-cymene in SAPRC-99). The SAPRC model program then lumped the species accordingly before running the simulation. For the MCM, species that are included explicitly in the mechanism were included, with other species mapped to the most appropriate similar compound.

The results for the headspace experiments are shown in Figures 18 and 19. The vapour used in these experiments contained primarily alkanes and alkenes with low amounts of aromatics. Ozone predictions were good for both SAPRC models, with SARPC-07 predicting somewhat less ozone than SAPRC-99. It is possible, given the uncertainty with regards to the HONO generation rate, that SAPRC-07 is modelling the experiment more effectively than SAPRC-99, but the reverse could also be true. However given the low impact of HONO generation on nitric oxide, both models can be said to predict nitric oxide loss very accurately. The MCM model did not predict these experiments as well as SAPRC, with lower ozone formation and a lower rate of nitric oxide loss simulated, however the amount of VOC reacted in MCM appears to be similar to that of SAPRC. Part of this difference between MCM and SAPRC can be attributed to the lumping of species in SAPRC, with isopentane (constituting 25% of total NMHC in these experiments) lumped into a group with a higher OH reaction rate than used for the individual compound in MCM.

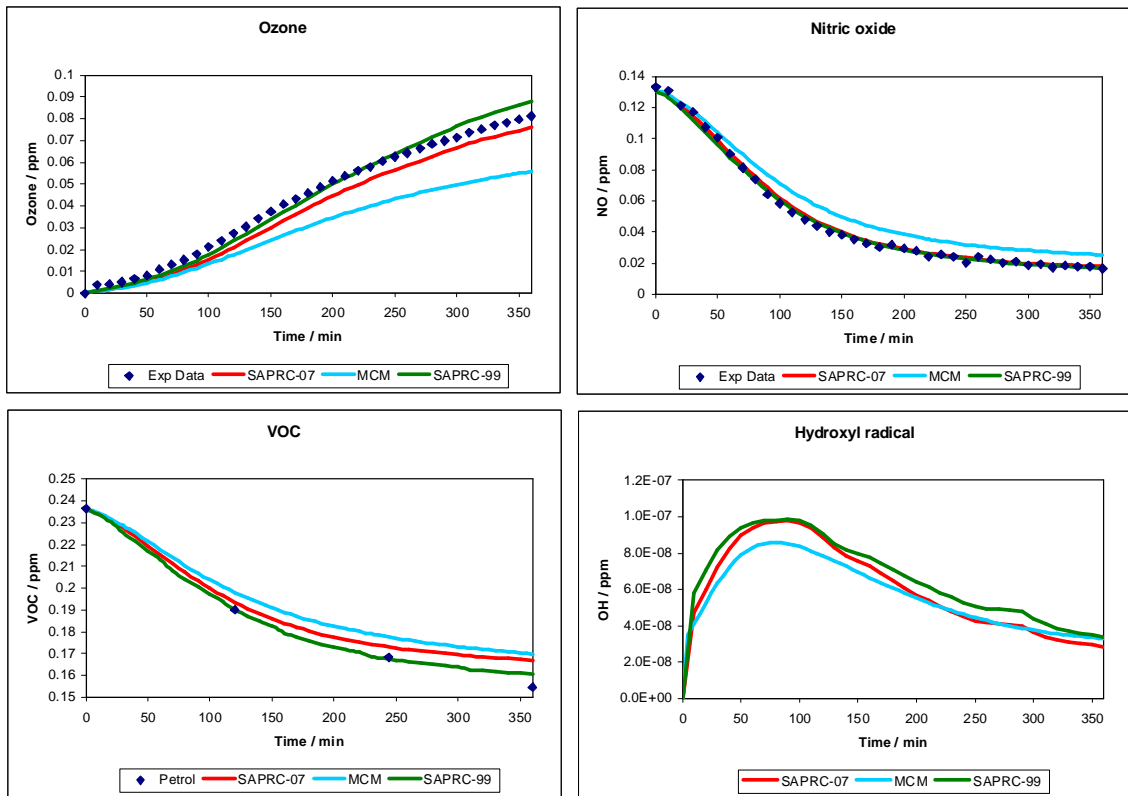


Figure 18: Modelled results for experiment 369 (ULP: 1149 ppbC; NO_x: 135 ppb; ROC/NO_x: 8.5)

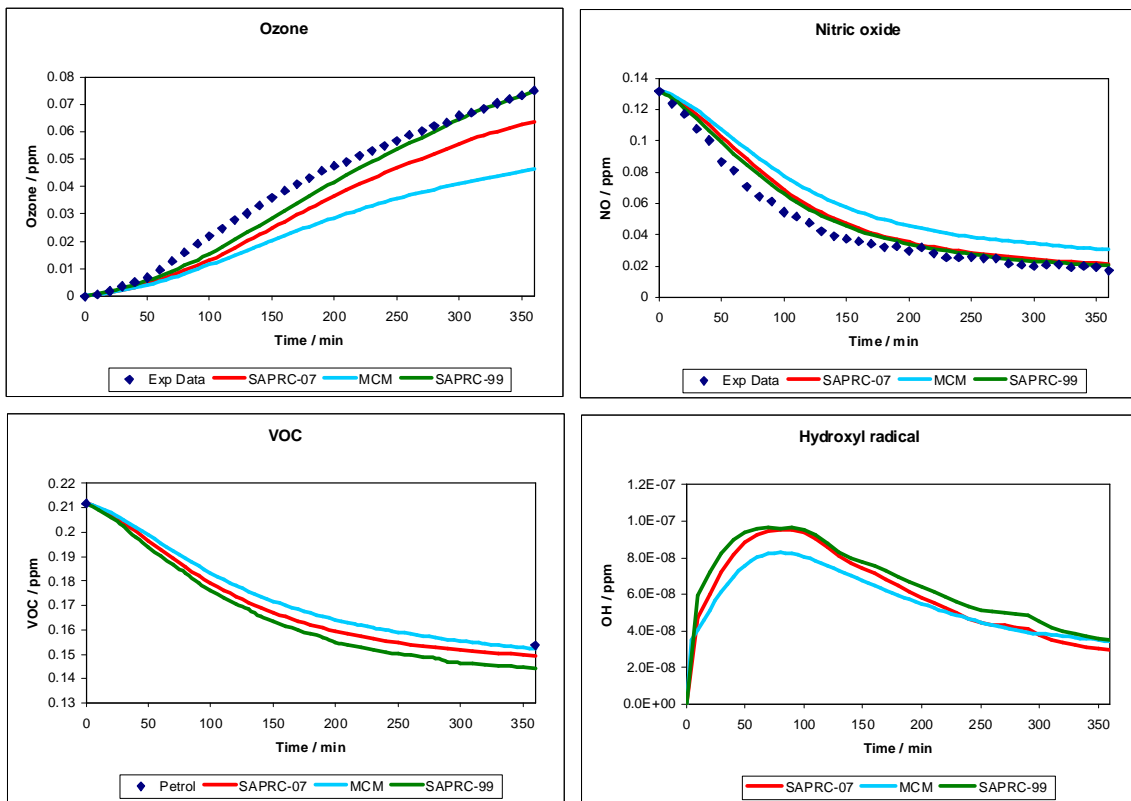


Figure 19: Modelled results for experiment 403 (ULP: 1044 ppbC; NO_x: 136 ppb; ROC/NO_x: 7.7)

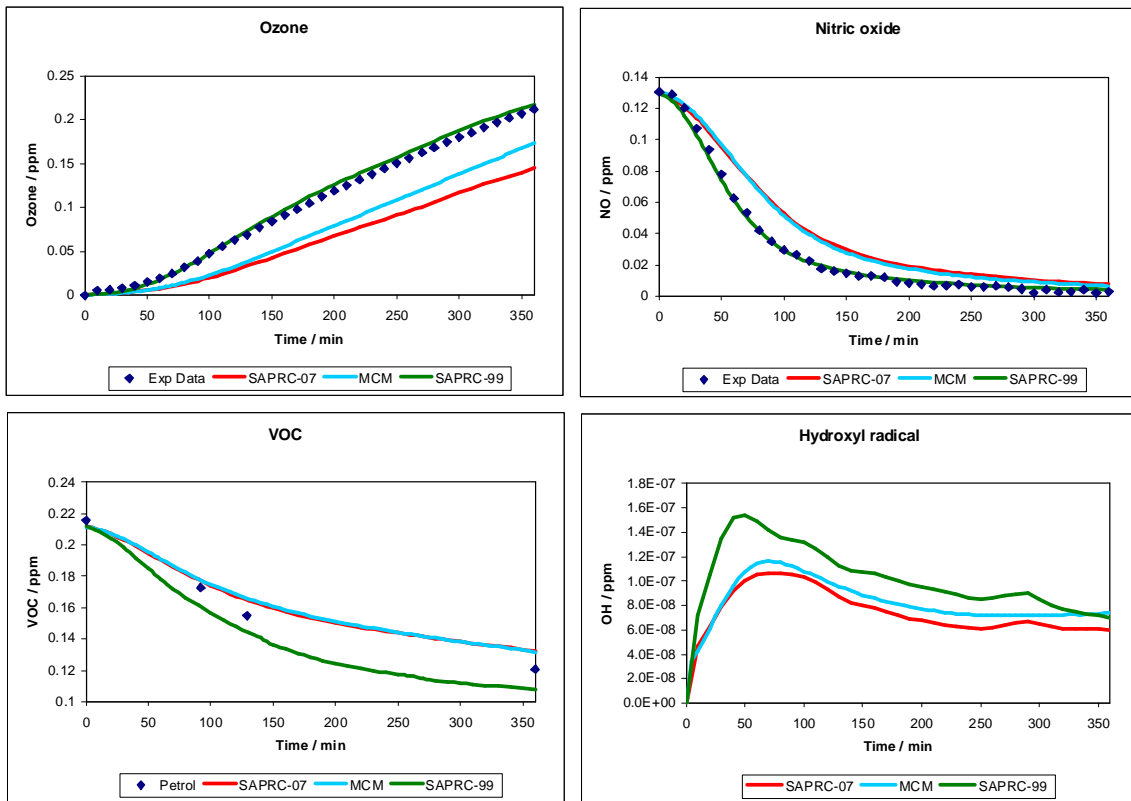


Figure 20: Modelled results for experiment 362 (ULP: 1401 ppbC; NO_x: 135 ppb; ROC/NO_x: 10.4)

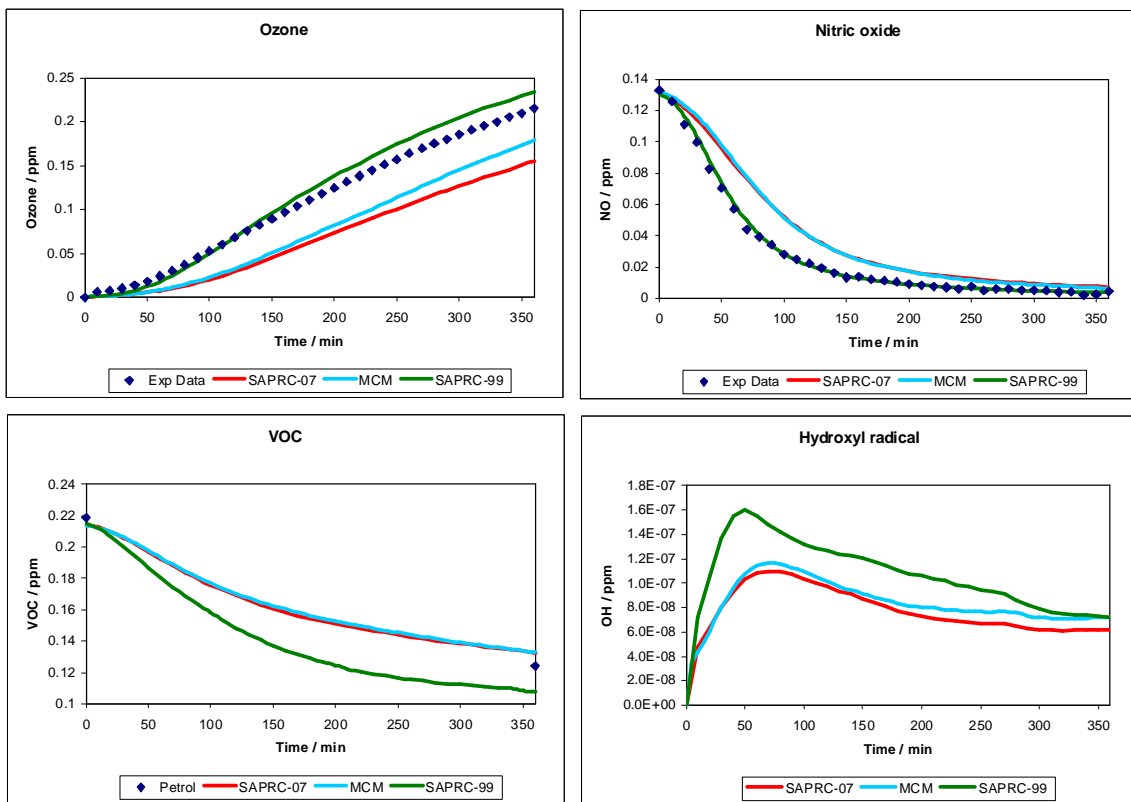


Figure 21: Modelled results for experiment 363 (ULP: 1420 ppbC; NO_x: 137 ppb; ROC/NO_x: 10.4)

The results for the wholly evaporated experiments are shown in Figures 20 and 21. These experiments contain a much higher concentration of aromatic species when compared to just the headspace experiments. For these experiments, ozone formation is again predicted quite accurately by SAPRC-99, but is underestimated by up to 40% by both MCM and SAPRC-07. This is reflected in the concentration profiles for OH and NO as well, with higher reactivity observed in the earlier SAPRC model. Importantly however, the concentration of VOC determined to have reacted using the SAPRC-99 model appears to be higher than what is observed experimentally, whereas MCM and SAPRC-07 predict slightly lower reaction of hydrocarbon species than observed. This indicates that the ozone formation is increased for SAPRC-99 as a result of higher hydrocarbon-OH reactions, which is likely given the higher OH concentrations observed in these simulations. These results are somewhat consistent with mixtures used in the evaluation of SAPRC-07, showing increased biases for $\Delta([O_3]-[NO])$ with experiments containing hydrocarbon mixtures (Carter 2008).

The one major difference that can be seen between the two varieties of ULP experiments is that the increase in aromatic species can cause large discrepancies in some chemical mechanisms. Another point worth highlighting is that during the wholly evaporated experiments secondary organic aerosol formed during the early stages of the experiment, whereas the headspace evaporated experiments formed no observable SOA after 6 hours. Aerosol formation is not considered in the chemical mechanisms evaluated here (although aerosol modules have been developed for them) and the effect this has on the chemistry has not been explored. Another issue with these experiments is the increased humidity used, as it is possible that the increased humidity will vary some of the key reaction rates forming radicals, in particular the auxiliary or wall mechanism.

While not included in this work, the formation of key species such as formaldehyde, carbon monoxide, PAN and nitric acid was predicted reasonably accurately for the ULP experiments. Formaldehyde and PAN in particular were estimated very accurately by all three models, whereas carbon monoxide was overpredicted by SAPRC-99 and underpredicted by SAPRC-07 for the wholly evaporated experiments.

3 CONCLUSIONS AND FURTHER WORK

The evaluation of the performance of the latest SAPRC-07 chemical mechanism in predicting the major photochemical smog oxidants was carried out using data collected from selected CSIRO smog chamber experiments. These experiments were carried out using *m*-xylene, toluene, isoprene and wholly evaporated and partially evaporated unleaded petrol (ULP). Predictions of ozone and other major oxidants for common set of initial conditions are compared to identify potential factors affecting the accuracy of each model simulations. Improvements have been made to SAPRC, such that it simulates more accurately the formation of key species during the single hydrocarbon-NO_x experiments evaluated in this study. However discrepancies between modelled and experimental data still exist for certain experimental scenarios, particularly in simulating the reaction of toluene and complex mixtures containing aromatic products.

The range of highly contaminant concentrations predicted by the selected mechanisms can be summarised as follows:

For single compounds:

- SAPRC-07 predicted the ozone formation from *m*-xylene sufficiently well, with a slight improvement observed when compared to SAPRC-99 predictions and a more considerable improvement over MCM predictions. The onset of ozone formation was modelled slightly early for experiments containing higher initial ROC/NO_x ratios, whereas for low ROC/NO_x experiments the rate of ozone formation was slower than observed.
- The rate of isoprene degradation and initial ozone formation was well predicted for all models tested, however, the mechanism failed to reproduce the timing and the magnitude of the transition from the hydrocarbon regime to the NO_x-limited conditions. This is believed to be related to the NO_y balance during this period, in particular the reactions of nitrogen-containing organic species.
- Oxidant formation from toluene was not well predicted by any model tested. SAPRC-07 in general predicted slightly better ozone profiles than SAPRC-99 or MCM, but the rate of ozone and other oxidant formation was much slower than observed for all experiments.

For wholly and partially evaporated ULP (gasoline):

- For wholly evaporated ULP, SAPRC-99 has predicted ozone formation and nitric oxide oxidation well, however SAPRC-99 also overestimated the hydrocarbon consumed during the experiment. SAPRC-07 underestimated ozone formation from wholly evaporated ULP when compared with SAPRC-99.
- For partially evaporated (headspace vapour) ULP, both SAPRC models predicted ozone formation well, as well as predicting VOC and NO oxidation accurately, however SAPRC-99 produced higher final ozone than SAPRC-07.
- The key difference between the wholly evaporated ULP vapour and headspace vapour experiments is that the concentration of aromatic species is significantly higher in the wholly evaporated ULP. This indicates that SAPRC-07 performs much better with hydrocarbon mixtures containing less aromatic hydrocarbons in highly reactive systems. This problem was not observed in SAPRC-99 for these experiments.

- For all experiments, MCM did not reproduce the observed ozone concentrations accurately, but was closer to observation for the more complex wholly evaporated ULP vapour than for the headspace vapour.

Further work is required to follow up on some of the issues encountered in this study:

- Investigation of the operators describing important radical chemistry (in particular RO_2) need to be evaluated for SAPRC-07 in comparison to SAPRC-99, given the extensive updates to the peroxy radical chemistry in the updated version.
- The only aromatics tested independently in this study were toluene and *m*-xylene. Other important aromatics that could be tested that would give a broader outlook to the ability of the model to predict aromatic photooxidation include *o*- and *p*-xylene, 1,2,4-trimethylbenzene, mesitylene, benzene and ethylbenzene.
- The impact that certain experimental conditions (such as photolysis rate, humidity and temperature) may have on model output could be tested by performing experiments which vary some of these conditions.
- Identifying specific reactions that are vital to the formation of important oxidants such as O_3 , NO_2 , HNO_3 and HCHO , and varying these reactions to assess their impact on the final simulated yields. Updates might then be made to better simulate experiments within the CSIRO chamber. Reactions of particular interest are the formation, thermal degradation, reaction and photolysis of nitrogen-containing organic species, as well as the reaction of aromatics to form important radicals such as HO_2 .
- Monitoring the concentrations of various hydrocarbons (or hydrocarbon classifications) rather than just the total hydrocarbon amount during the ULP experiments, which can be used to assess the updates made to the MIR values for SAPRC-07. Further experimental work is also required on hydrocarbon mixtures, particularly in determining which species are not well accounted for in modelling the reactions of complex mixtures, and in experiments in which no external radical source is added.

4. ACKNOWLEDGEMENTS

We are grateful to the Department of the Environment, Water, Heritage and the Arts (DEWHA) for making the data available and to CSIRO for allowing the current review to proceed. We would like to acknowledge Dr John Carras, Dr Martin Cope and Dr Ian Jamie for their helpful discussions, Dr Lila Singh, Michael Patterson and Peter Nancarrow for their contribution and assistance with smog chamber experiments and Dr Graeme Batley for reviewing this report.

5. REFERENCES

- Allen, G., Remedios, J.J., Newnham, D.A., Smith, K.M., Monks, P.S., 2005. Improved mid-infrared cross-sections for peroxyacetyl nitrate (PAN) vapour. *Atmospheric Chemistry and Physics* 5, 47-56.
- Angove, D.E., Fookes, C.J.R., Hynes, R.G., Walters, C.K., Azzi, M., 2006. The characterisation of secondary organic aerosol formed during the photodecomposition of 1,3-butadiene in air containing nitric oxide. *Atmospheric Environment* 40, 4597-4607.
- Bloss, C., Wagner, V., Jenkin, M.E., Volkamer, R., Bloss, W.J., Lee, J.D., Heard, D.E., Wirtz, K., Martin-Reviejo, M., Rea, G., Wenger, J.C., Pilling, M.J., 2005. Development of a detailed chemical mechanism (MCMv3.1) for the atmospheric oxidation of aromatic hydrocarbons. *Atmospheric Chemistry and Physics* 5, 641-664.
- Bloss, C., Wagner, V., Bonzanini, A., Jenkin, M.E., Wirtz, K., Martin-Reviejo, M., Pilling, M.J., 2005a. Evaluation of detailed aromatic mechanisms (MCMv3 and MCMv3.1) against environmental chamber data. *Atmospheric Chemistry and Physics* 5, 623-639.
- Carter, W.P.L., 2000. Documentation of the SAPRC-99 chemical mechanism for VOC reactivity assessment. Report to the California Air Resources Board, Contracts 92-329 and 95-308, May 8.
- Carter, W.P.L., 2008. Development of the SAPRC-07 chemical mechanism and updated ozone reactivity scales. Final Report to the California Air Resources Board, Contract 03-318, July 7.
- Carter, W.P.L., Lurmann, F.W., 1991. Evaluation of a detailed gas-phase atmospheric reaction mechanism using environmental chamber data. *Atmospheric Environment* 25A, 2771-2806.
- Carter, W.P.L., Atkinson, R., Winer, A.M., Pitts Jr., J.N., 1982. Experimental Investigation of Chamber-Dependent Radical Sources. *International Journal of Chemical Kinetics* 14, 1071-1103.
- Chu, P.M., Guenther, F.R., Rhoderick, G.C., Lafferty, W.J. 1999. The NIST Quantitative Infrared Database. *Journal of research of the National Institute of Standards and Technology* 104, 59-81. Available at website: <http://webbook.nist.gov/chemistry/quant-ir/>
- Febo, A., Perrino, C., Gherardi, M., Sparapani, R., 1995. Evaluation of a high-purity and high-stability continuous generation system for nitrous acid. *Environmental Science and Technology* 29, 2390-2395.
- Finlayson-Pitts, B.J., Wingen, L.M., Sumner, A.L., Syomin, D., Ramazan, K.A., 2003. The heterogeneous hydrolysis of NO₂ in laboratory systems and in outdoor and indoor atmospheres: An integrated mechanism. *Physical Chemistry Chemical Physics* 5, 223-242.
- Fuzzi, S., Andreae, M.O., Huebert, B.J., Kulmala, M., Bond, T.C., Boy, M., Doherty, S.J., Guenther, A., Kanakidou, M., Kawamura, K., Kerminen, V.-M., Lohmann, U., Russell, L.M., Pöschl, U., 2006. Critical assessment of the current state of scientific knowledge, terminology, and research needs concerning the role of organic aerosols in the atmosphere, climate, and global change. *Atmospheric Chemistry and Physics* 6, 2017-2038.
- Hanst, P.L., Hanst, S.T., 1993. *Infrared Spectra for Quantitative Analysis of Gases*, Infrared Analysis, Inc., Anaheim, CA. Available at website: <http://www.infraredanalysisinc.com/>

Hynes, R.G., Angove, D.E., Saunders, S.M., Haverd, V., Azzi, M., 2005. Evaluation of two MCM v3.1 alkene mechanisms using indoor environmental chamber data. *Atmospheric Environment* 39, 7251-7262

IUPAC, 2006. Evaluated Kinetic and Photochemical Data. IUPAC Subcommittee on Gas Kinetic Data Evaluation for Atmospheric Chemistry. Web Version October 2006. Available at website: <http://www.iupackinetic.ch.cam.ac.uk>

Mallet, V., Sportisse, B., 2006. Uncertainty in a chemistry-transport model due to physical parameterizations and numerical approximations: An ensemble approach applied to ozone modelling. *Journal of Geophysical Research* 111, D01302

Metzger, A., Dommen, J., Gaeggler, K., Duplissy, J., Prevot, A.S.H., Kleffmann, J., Elshorbany, Y., Wisthaler, A., Baltensperger U., 2008. Evaluation of 1,3,5-trimethylbenzene degradation in the detailed tropospheric chemistry mechanism, MCMv3.1, using environmental chamber data. *Atmospheric Chemistry and Physics* 8, 6453-6468.

NASA, 2006. Chemical Kinetics and Photochemical Data for Use in Atmospheric Studies, Evaluation Number 15. JPL Publication 06-2, Jet Propulsion Laboratory, California Instituted of Technology, Pasadena, California. Available at website: <http://jpldataeval.jpl.nasa.gov/>

Rohrer, F., Bohn, B., Brauers, T., Bruning, D., Johnen, F.-J, Wahner, A., Kleffman, J., 2005. Characterisation of the photolytic HONO-source in the atmosphere simulation chamber SAPHIR. *Atmospheric Chemistry and Physics* 5, 2189-2201.

Tadić, J., Moortgat, G.K., Wirtz, K., 2006. Photolysis of glyoxal in air. *Journal of Photochemistry and Photobiology A: Chemistry* 177, 116-124.

Zador, J., Turanyi, T., Wirtz, K., Pilling, M.J., 2006. Measurement and investigation of chamber radical sources in the European Photoreactor (EUPHORE). *Journal of Atmospheric Chemistry* 55, 147-166.

This page was intentionally left blank

APPENDIX A: AUXILIARY MECHANISM

In order to effectively simulate atmospheric processes in environmental chambers, the effect of the surfaces in generating radicals must be understood. These effects include chamber radical sources, the decay of inorganic compounds (NO_x , O_3), chamber dilution and the effect of background organic species. The most important of these are the radicals formed from the chamber walls, which have been attributed to a chamber radical source (A1) (Carter et al. 1982) and NO_x offgassing (A2) (Carter and Lurmann 1991).



Recent studies, though, indicate that these two reactions can be better approximated using the offgassing of HONO (3), which has been observed in reasonable concentration as a product of surface wall reactions in smog chambers (Rohrer et al. 2004, Metzger et al. 2008)



For the CSIRO smog chamber, an auxiliary mechanism for modelling with MCM was developed by Hynes et al. (2005), as shown in Table A1.

Table A1: Auxiliary mechanism as described in Hynes et al. (2005)

Reaction	Parameter
$h\nu + \text{wall} \rightarrow \text{OH}$	$J_{\text{NO}_2} (0.0015) \text{ ppb s}^{-1}$
$h\nu + \text{wall} \rightarrow \text{NO}_2$	$J_{\text{NO}_2} (0.0015) \text{ ppb s}^{-1}$
$\text{NO}_2 \rightarrow 0.5 \times (\text{HONO} + \text{wHNO}_3)$	$1 \times 10^{-6} \text{ s}^{-1}$
$\text{N}_2\text{O}_5 \rightarrow 2 \times \text{wHNO}_3$	$1 \times 10^{-5} \text{ s}^{-1}$
$\text{N}_2\text{O}_5 + \text{H}_2\text{O} \rightarrow 2 \times \text{wHNO}_3$	$1 \times 10^{-20} \text{ cm}^3 \text{ molecule}^{-1} \text{ s}^{-1}$
$h\nu + \text{wHNO}_3 \rightarrow \text{OH} + \text{NO}_2$	J_{HNO_3}
$\text{HNO}_3 \rightarrow \text{wHNO}_3$	$1 \times 10^{-4} \text{ s}^{-1}$
$\text{NO}_2 \rightarrow \text{wall}$	$2 \times 10^{-7} \text{ s}^{-1}$
$\text{O}_3 \rightarrow \text{wall}$	$2 \times 10^{-7} \text{ s}^{-1}$

However, the chamber radical source can vary over time from chamber usage (Carter et al. 2005) and as such some aspects of the auxiliary mechanism were re-evaluated. Also, due to varying photolysis and reaction rates of important inorganic species between the three models evaluated (SAPRC-07, SAPRC-99 and MCMv3.1), independent auxiliary mechanisms were developed.

The initial background species (CO and CH_4) were estimated in the previous characterisation experiments because their absolute initial concentrations were not easy to obtain. So while the estimated values were close to what are typically measured in the chamber presently, the long path FT-IR cell can provide reasonably accurate initial concentrations which have been included in the various simulations listed here.

NO_x offgassing

The radical source and NO_x offgassing was attributed to equations (A1) and (A2) above, however in this work it was decided to use the offgassing of HONO (A3) to best represent this source. For two CO-air experiments at $J_{\text{NO}_2} = 0.39 \text{ min}^{-1}$, it was found that a rate equal to:

$$J_{\text{NO}_2} \times 0.004 \text{ ppb s}^{-1}$$

best approximated ozone formation for all three models. While the NO_x offgassing is believed to be temperature and humidity dependent, the majority of these experiments were performed using similar temperature regimes (initial $296 \pm 2 \text{ K}$ and final $304 \pm 4 \text{ K}$) and similarly low humidity (between 2-5 %RH at 293 K), so it is concluded that this rate is applicable for experiments performed under those conditions.

Chamber radical source

Chamber experiments were also performed using CO-NO_x mixtures. However, problems arose in using these mixtures as aerosol of diameter approximately 50 nm formed upon the injection of NO_x but before experiment initiation. It is believed that the increase in aerosol number (as well as a small increase in aerosol number observed in CO-air experiments) is due to the specific CO source used, and the aerosol material is likely to be metallic in nature arising from the gas cylinder. While this will undoubtedly have an effect on the gas phase chemistry, it is believed that most of this aerosol is not organic since an ice cold trap was used during CO injection and the effective aerosol surface area is much less than the chamber walls. Comparison of the rates established by CO-NO_x experiment can be compared to clean air photolysis experiments to see if they are valid in non-CO experiments.

Using the NO_x offgassing rate found above, it was found to be insufficient in modelling ozone formation from CO-NO_x and clean air experiments, with the ozone modelled about half of that observed. The addition of a direct chamber radical source (A1) was also found not to work, as it overestimated the ozone formation from CO-air experiments. The solution appeared to be the use of excess hydrocarbon reactivity (XSHC in SAPRC) which converts OH to HO₂. The subsequent reaction of HO₂ with NO forms NO₂, which in turn is photolysed to form ozone.



This effect had been accounted for in the previous characterisation by measurement of the background hydrocarbons themselves, and the inclusion of these molecules in the mechanism. While this provides a much more accurate mechanism for predicting other products of oxidation (such as formaldehyde), the inclusion of an excess hydrocarbon term is more effective for characterising background effects in the chamber where background hydrocarbons have not been measured.

For the various models, the reaction rate of equation (A4) that best fits ozone formation was found to be:

SAPRC-07:	$2.0 \times 10^3 \text{ min}^{-1}$
SAPRC-99:	$8.0 \times 10^2 \text{ min}^{-1}$
MCM:	$3.0 \times 10^3 \text{ min}^{-1}$ (represented as $5.0 \times 10^1 \text{ s}^{-1}$)

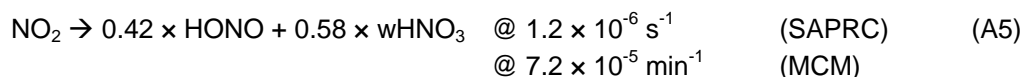
The reasons why different reactions rates are required for the same reaction in different models are believed to be related to the reaction rates for HO₂ and OH with NO_x. Adding excess hydrocarbon has little effect on the CO-air experiments, but models ozone formation during clean air photolysis experiments well. However, these values are particularly high and are probably indicative of background aerosol effects for CO-NO_x experiments, and high background hydrocarbon for some of the clean air experiments. Using these parameters to model *m*-xylene experiments found that the XSHC values above biased the model towards high ozone (whereas the ozone values modelled with a

negligible XSHC term for *m*-xylene predicted ozone much more accurately). Therefore, in line with other chamber auxiliary mechanisms, the rates were fixed at:

SAPRC-07 & SAPRC-99:	250 min ⁻¹
MCM:	4 sec ⁻¹ (effectively 240 min ⁻¹)

NO₂ reactions

The wall reactions involving NO₂ in the chamber were limited in this chamber to the dry deposition of NO₂ to form HONO and wall-deposited NO_x (represented by wHNO₃), and the direct loss of NO₂. The hydrolysis of NO₂ on surfaces was studied by Finlayson-Pitts et al. (2003) showing the formation of HONO (and NO on an acidic surface) in yields around 50% at low concentrations of varying humidity. The rate of reaction is dependent on both the surface used and the humidity. Given that nearly all experiments here are performed at less than 5% relative humidity and J_{NO2} between 0.39 and 0.46 min⁻¹, the reaction of NO₂ on the walls has been left as light and humidity independent and is the combination of both terms. Also, the reaction being a dark deposition term is assumed to be equivalent in each model, and the difference between calculating on different time intervals insignificant, such that:



Reactions of O₃ and N₂O₅

The reactions of these species have been left as they were reported previously.

Reactions of wHNO₃

Previously, the deposition of nitric acid was assumed to occur at a considerably high rate (1.0 × 10⁻⁴ s⁻¹), and this rate was determined by monitoring the nitric acid concentration in butadiene-NO_x experiments. However, given the high concentrations of HNO₃ present during aromatic-NO_x experiments in the CSIRO chamber (often in excess of 40 ppb at the end of an experiment) and the low relative photolysis rate of HNO₃ in black light chambers, this rate can remove a high proportion of the observed NO_y. To test the actual dark deposition of HNO₃, nitric acid was injected into the chamber by passing nitrogen through a nitric acid-water solution of pH 2. The nitric acid vapour of undetermined concentration (see below) was left in the chamber in the dark for 3 hours, and after this time, the chamber lights were activated for 2 hours, before being left in the dark for one hour.

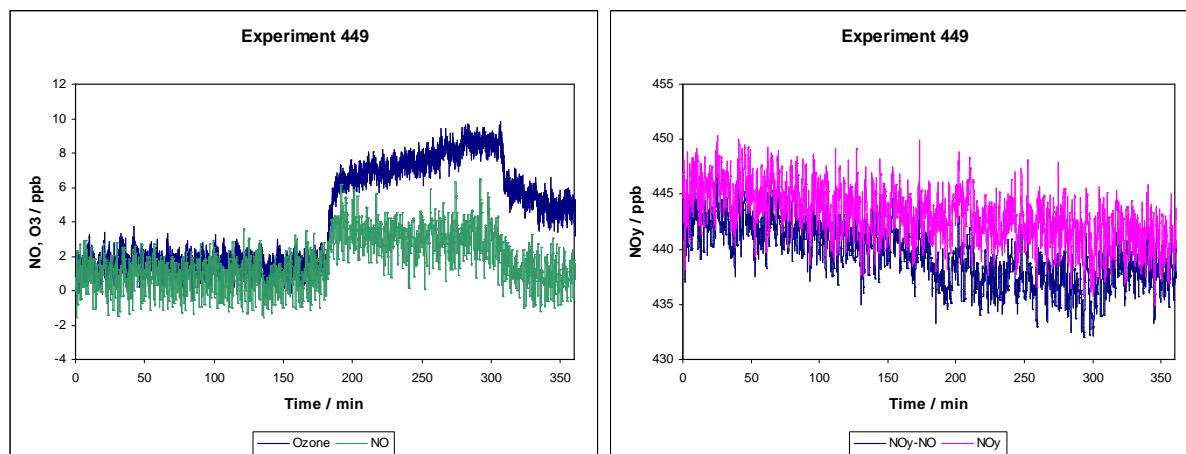


Figure A1: Experiment profile for nitric acid experiment.

During the dark period, ozone and NO remained constant while the observed NO_y (as measured using chemiluminescence) decreased gradually (Figure A1). After the lights were turned on, a quick equilibrium was observed, with the amount of ozone and NO increasing, indicative of reactions expected with a small amount of NO_2 being present in the chamber. Ozone steadily increased during photolysis while NO remained relatively constant, quite likely due to the reaction and photolysis of HNO_3 to form small quantities of NO_2 (as well initial NO_2 that may have been formed as a minor side product during injection of HNO_3 into the chamber). After the lights were turned off, an equilibrium was formed again, such that all available NO quickly reacted with ozone, leaving a small amount of excess ozone formed during photolysis. The total amount of observable NO_y decreased steadily during both the dark and light phases, with no observable difference in rate, losing approximately 5 ppb across the experiment.

Nitric acid was observed during the experiment using FT-IR measurements (Figure A2). The amounts shown on the y-axis of Figure A2 are indicative only, as quantification of nitric acid reference spectra was problematic. However, the nitric acid loss was found to be first order during both dark and light periods, at rates of $3.3 \times 10^{-6} \text{ s}^{-1}$ and $4.5 \times 10^{-6} \text{ s}^{-1}$ respectively. The latter value will also include other reactions (such as photolysis or removal by OH), so using the dark rate is sufficient for actual nitric acid wall loss. The fate of nitric acid remains unclear, although it is believed to form HONO or NO_2 . As the NO_y detected decreases slightly, it is likely that nitric acid is indeed lost to the wall during experiment, but quantification of the nitric acid is required to determine the exact concentration and equivalent yields of products.

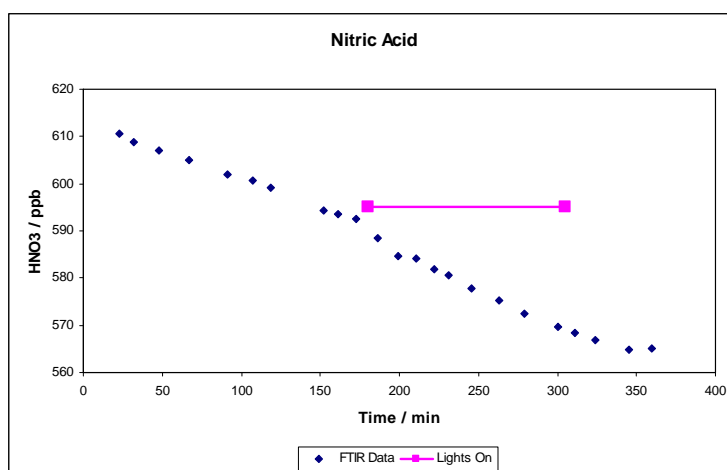


Figure A2: Nitric acid as observed using FTIR for experiment 449

For modelling purposes, the dark deposition rate of HNO_3 was used, while the $w\text{HNO}_3$ photolysis term was removed. While it is likely that the wall-bound nitric acid does form gaseous nitrogen species from photolysis, the J_{HNO_3} rate for a black light chamber is considerably low that removing it has little impact on the chemistry.

Existing problems with auxiliary mechanism

The effect of formaldehyde offgassing or wall loss has not been included, but was found previously to be sufficiently small to ignore in the CSIRO chamber (Hynes et al. 2005). Most importantly the impact of temperature and water content on the auxiliary mechanism has not been accounted for here, despite it having a non-negligible impact on radical sources (Carter et al. 2005, Zador et al. 2006). However, given the relatively stable temperature after 40 minutes and similarly low humidity in most experiments here, the mechanism is considered valid for experiments performed under these conditions.

The wall mechanism as of this stage for the three models tested is listed in Table A2.

Table A2: Auxiliary mechanism as used for CSIRO chamber

Reaction	SAPRC-term	SAPRC-07	SAPRC-99	MCM v3.1
$h\nu + \text{wall} \rightarrow \text{HONO}$	RN-I ($\times J_{\text{NO}_2}$)	$J_{\text{NO}_2} \times (4 \times 10^{-6})$ ppm	$J_{\text{NO}_2} \times (4 \times 10^{-6})$ ppm	$J_{\text{NO}_2} \times (4 \times 10^{-3})$ ppb
$\text{NO}_2 \rightarrow \alpha \times \text{HONO} + (1 - \alpha) \times \text{wNO}_x$	K(NO2)W	$7.2 \times 10^{-5} \text{ min}^{-1}$	$7.2 \times 10^{-5} \text{ min}^{-1}$	$1.2 \times 10^{-6} \text{ s}^{-1}$ ($7.2 \times 10^{-5} \text{ min}^{-1}$)
α	y-HONO	0.42	0.42	0.42
$\text{N}_2\text{O}_5 \rightarrow 2 \times \text{wNO}_x$	K(N25I)	$6.0 \times 10^{-4} \text{ min}^{-1}$	$6.0 \times 10^{-4} \text{ min}^{-1}$	$1.0 \times 10^{-5} \text{ s}^{-1}$ ($6.0 \times 10^{-4} \text{ min}^{-1}$)
$\text{N}_2\text{O}_5 + \text{H}_2\text{O} \rightarrow 2 \times \text{wNO}_x$	K(N25S)	$1.48 \times 10^{-5} \text{ ppm}^{-1} \text{ min}^{-1}$	$1.48 \times 10^{-5} \text{ ppm}^{-1} \text{ min}^{-1}$	$*[\text{H}_2\text{O}] \times 10^{20} \text{ cm}^3$ $\text{molecule}^{-1} \text{ s}^{-1}$
$\text{O}_3 \rightarrow \text{wall}$	K(O3)W	$1.2 \times 10^{-5} \text{ min}^{-1}$	$1.2 \times 10^{-5} \text{ min}^{-1}$	$2.0 \times 10^{-7} \text{ s}^{-1}$ ($1.2 \times 10^{-5} \text{ min}^{-1}$)
$\text{OH} \rightarrow \text{HO}_2$	XSHC	$2.5 \times 10^2 \text{ min}^{-1}$	$2.5 \times 10^2 \text{ min}^{-1}$	4.0 s^{-1} ($2.4 \times 10^2 \text{ min}^{-1}$)
$\text{HNO}_3 \rightarrow \text{wNO}_x$	K(NAW)	$1.98 \times 10^{-4} \text{ min}^{-1}$	$1.98 \times 10^{-4} \text{ min}^{-1}$	$3.3 \times 10^{-6} \text{ s}^{-1}$ ($1.98 \times 10^{-4} \text{ min}^{-1}$)
$\text{wHNO}_3 \rightarrow \text{NO}_2 + \text{OH}$	-	-	-	-

* Effective rate = $[\text{H}_2\text{O}] \times 6.0 \times 10^{19} \text{ cm}^3 \text{ molecule}^{-1} \text{ min}^{-1}$

Initial HONO

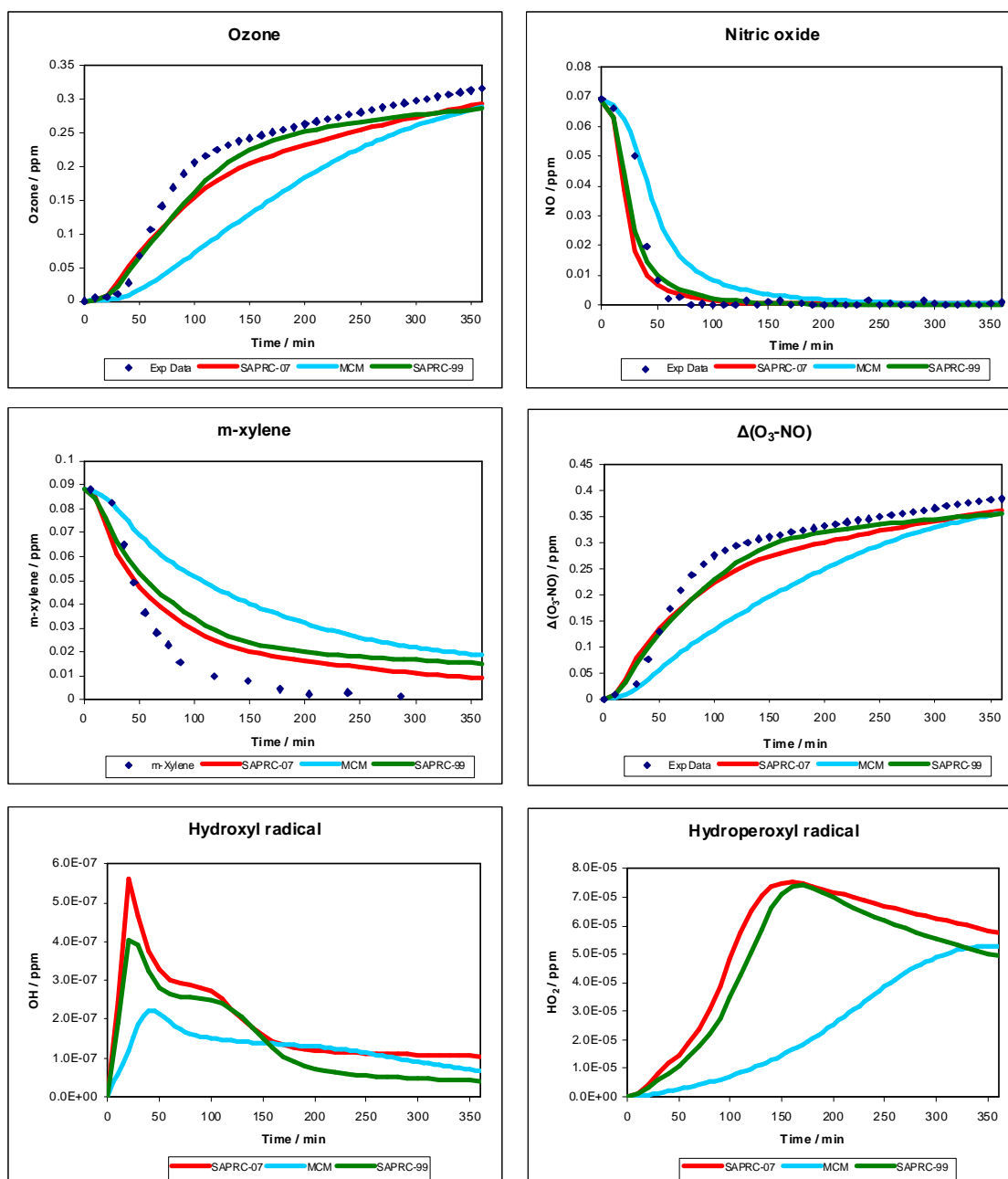
Once the above auxiliary mechanism was inserted, it was found that the rate of oxidation during isoprene- NO_x experiments was very dependent on the initial HONO specified for each experiment using all models. Using SAPRC-07, the initial HONO could be varied such that the simulated ozone matched the observed ozone (until NO levels became low), or alternatively that the simulated NO could be matched to the observed values. It was found that the two were not equivalent, matching ozone required 30-50% higher initial HONO than the matching of NO. Given that initial NO_2 concentration is likely linked to the initial amount of NO used, and initial HONO concentration is similarly related to NO_2 , the initial HONO concentration could be linked to initial NO_x (measured in ppb) by equation (A6).

$$[\text{HONO}]_0 = 0.1 + (3.3 \times 10^{-3} [\text{NO}_x]_0) \text{ ppb} \quad (\text{A6})$$

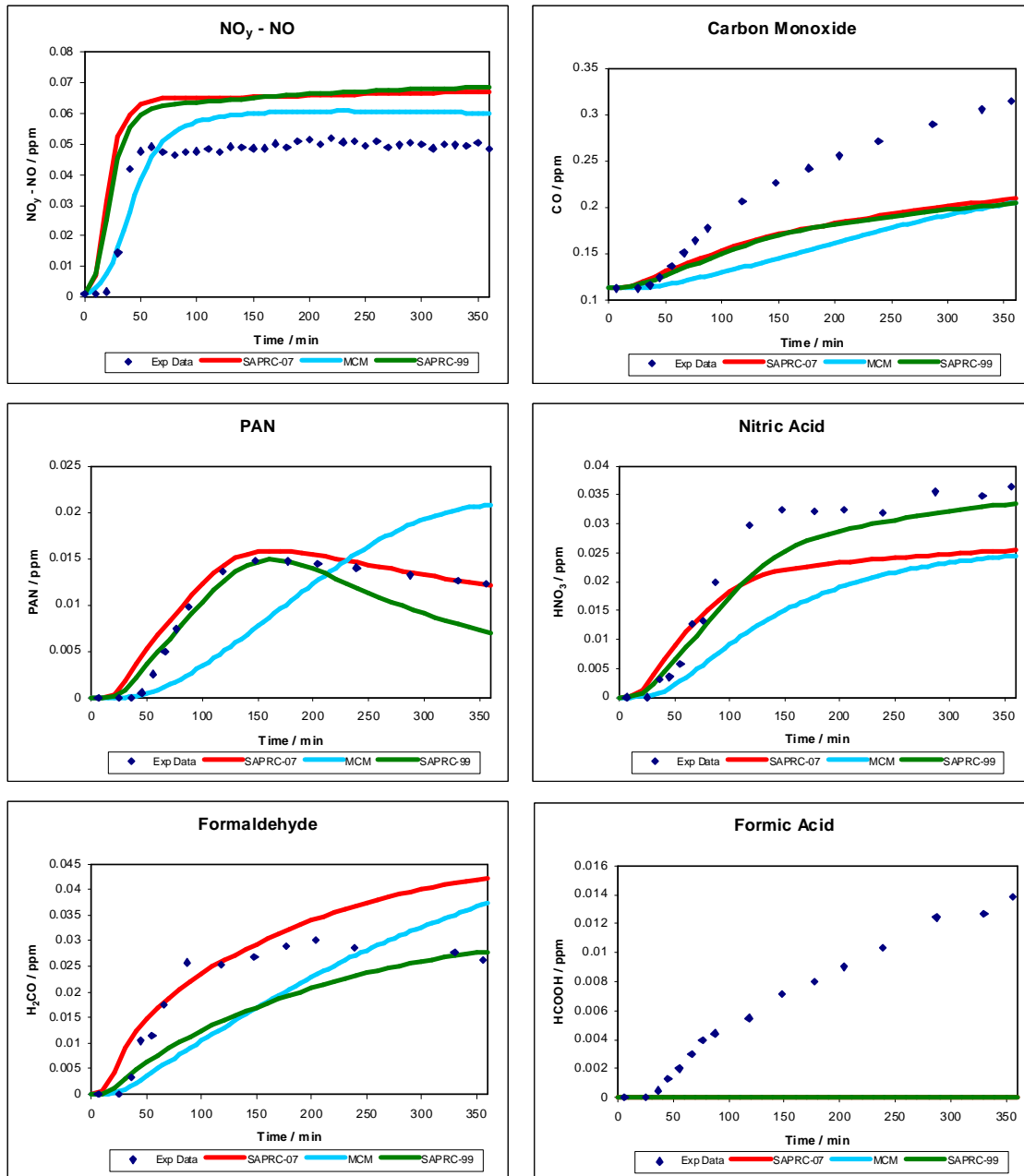
The amount of HONO is added to the initial NO and NO_2 in all cases, rather than being subtracted from the initial NO_x concentration.

APPENDIX B: M-XYLENE EXPERIMENT RESULTS

Experiment : 416					
Initial Conditions:			ROC/NO _x	10.06	
NO	69	ppbv	HONO	0.34	ppbv
NO ₂	1	ppbv	J _{NO2}	0.43	min ⁻¹
CO	112	ppbv	HONO gen	0	ppbv hr ⁻¹
m-xylene	88	ppbv	Initial Temp	296.75	°K
CH ₄	1.5	ppmv	Max Temp	304.35	°K
H ₂ O	782	ppmv	Final Temp	304.05	°K

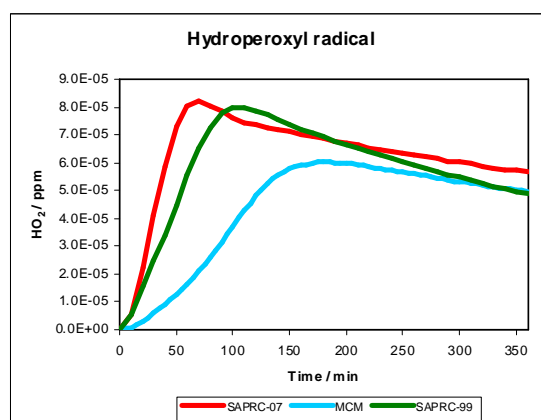
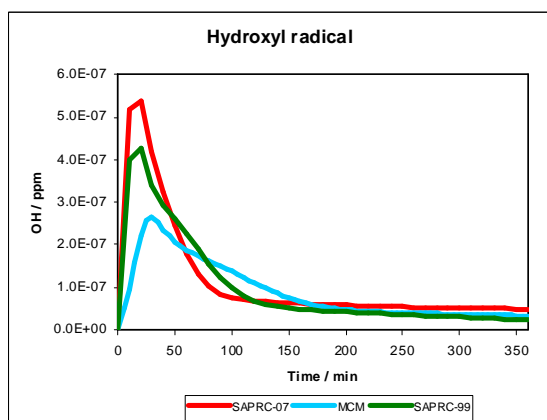
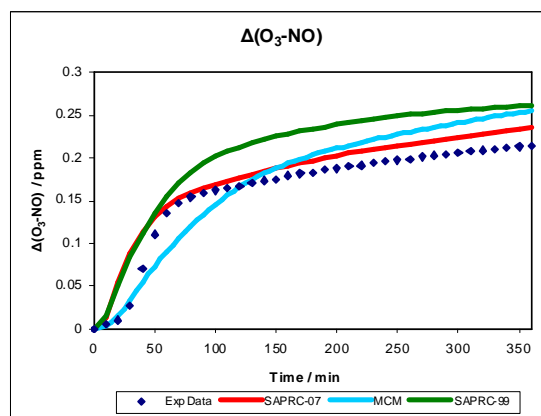
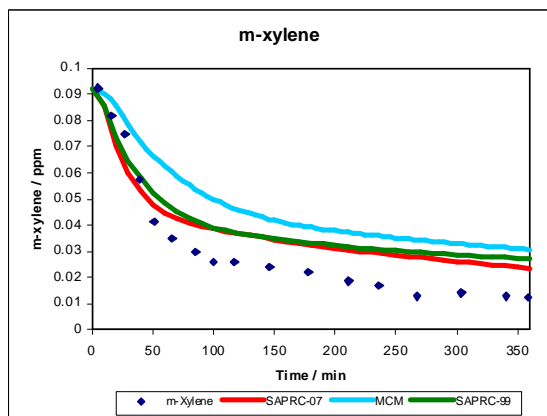
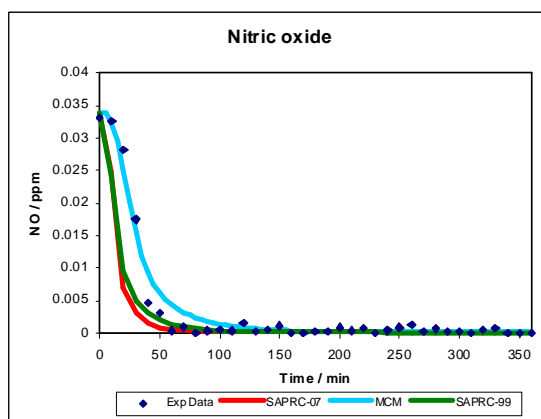
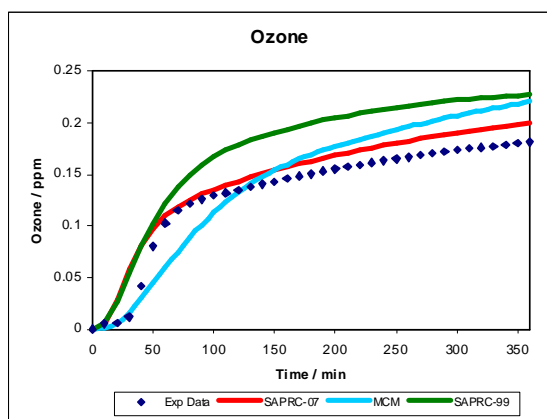


Appendix B1: Modelled results for experiment 416

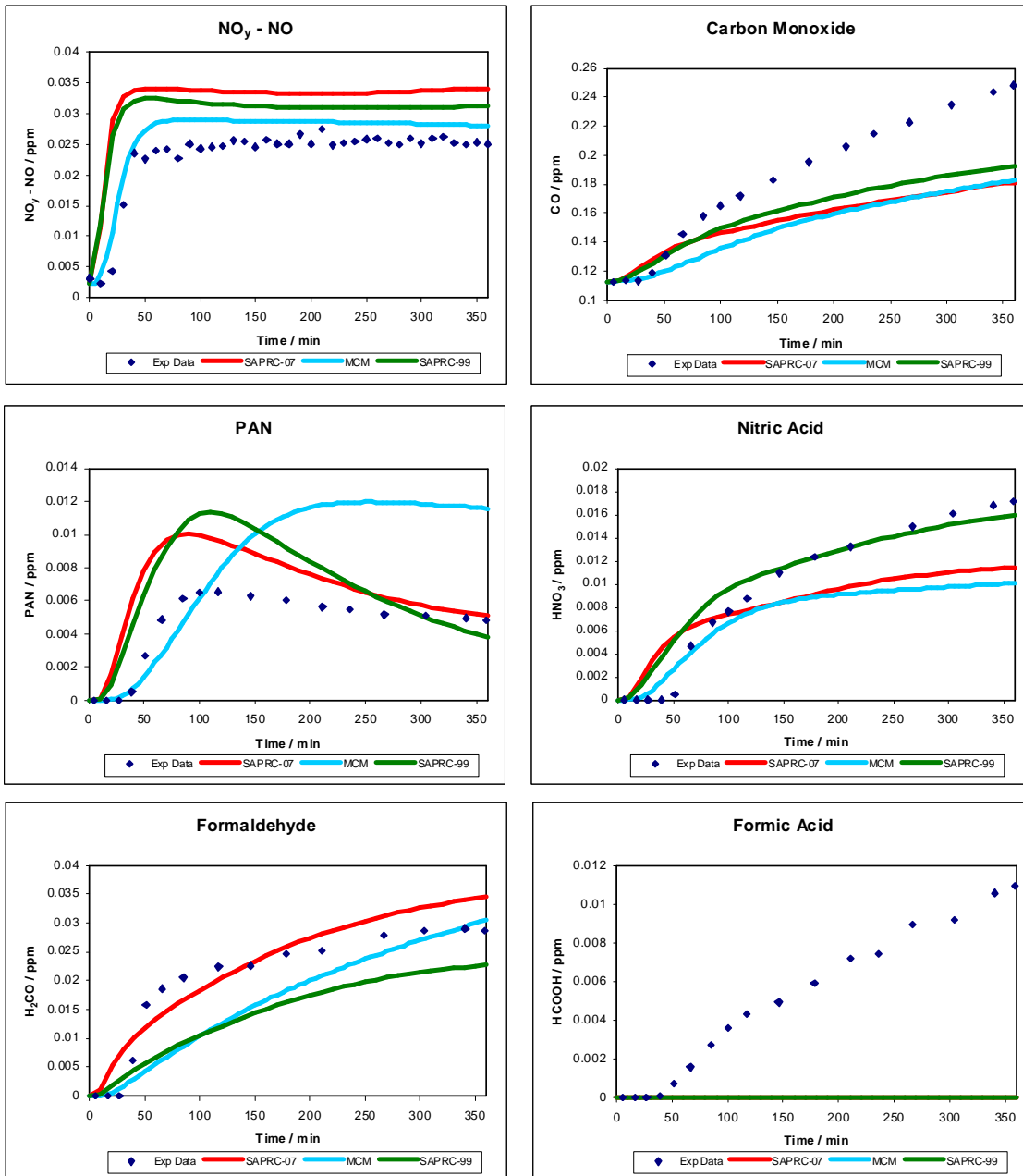


Appendix B1 (cont.): Modelled results for experiment 416

Experiment : 428					
Initial Conditions:			ROC/NO _x	20.44	
NO	34	ppbv	HONO	0.23	ppbv
NO ₂	2	ppbv	J _{NO2}	0.43	min ⁻¹
CO	113	ppbv	HONO gen	0	ppbv hr ⁻¹
m-xylene	92	ppbv	Initial Temp	295.3	°K
CH ₄	1.45	ppmv	Max Temp	304.55	°K
H ₂ O	1304	ppmv	Final Temp	303.9	°K



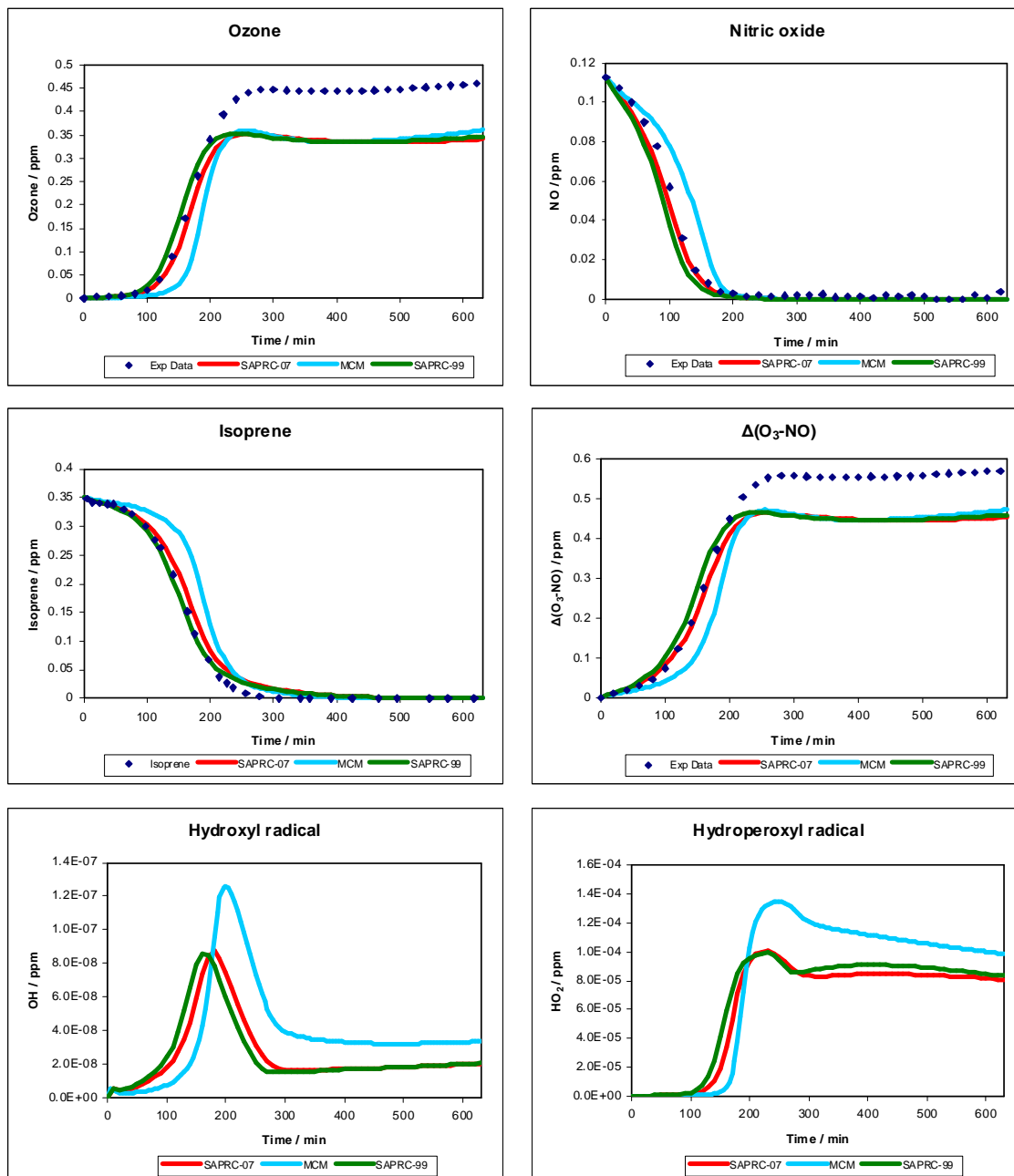
Appendix B2: Modelled results for experiment 428



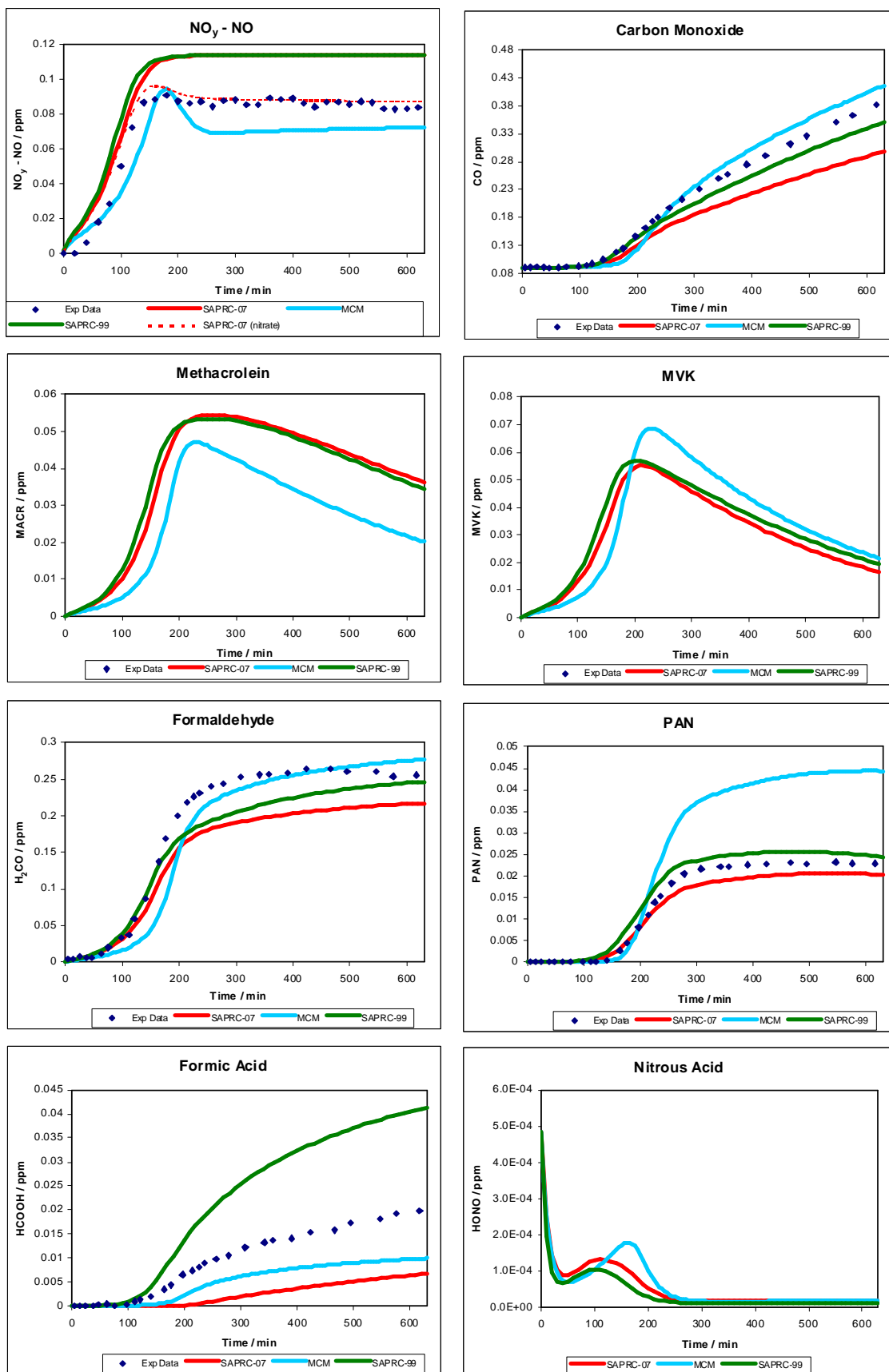
Appendix B2 (cont.): Modelled results for experiment 428

APPENDIX C: ISOPRENE EXPERIMENT RESULTS

Experiment : 303					
Initial Conditions:			ROC/NO _x	15.35	
NO	113	ppbv	HONO	0.49	ppbv
NO ₂	1	ppbv	J _{NO2}	0.41	min ⁻¹
CO	90	ppbv	HONO gen	0	ppbv hr ⁻¹
Isoprene	350	ppbv	Initial Temp	294.1	°K
CH ₄	1.5	ppmv	Max Temp	301.9	°K
H ₂ O	1000	ppmv	Final Temp	301.9	°K

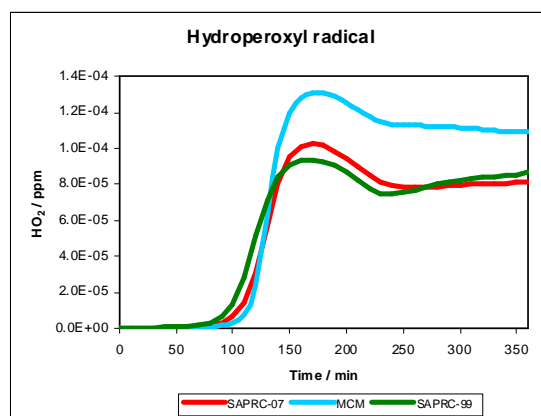
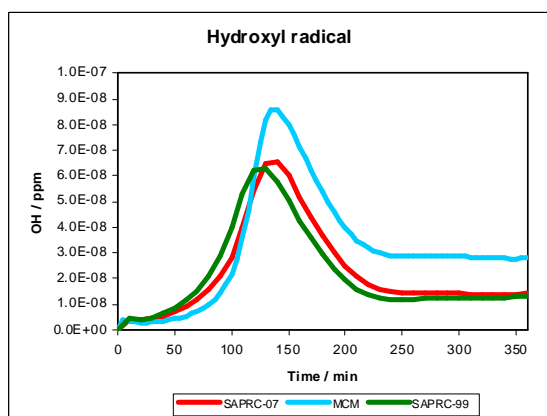
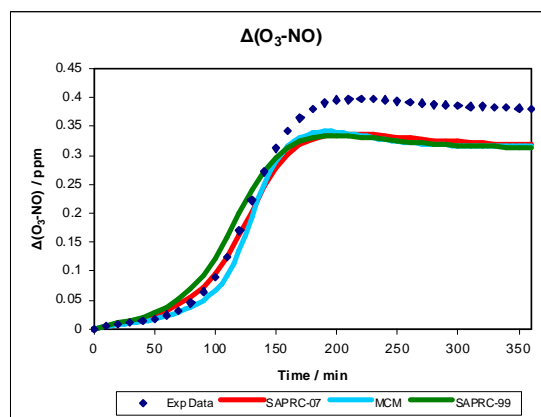
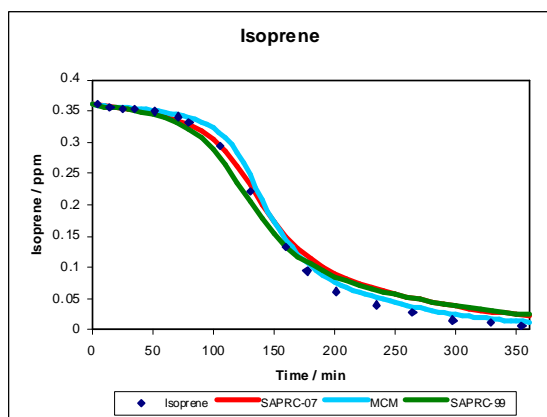
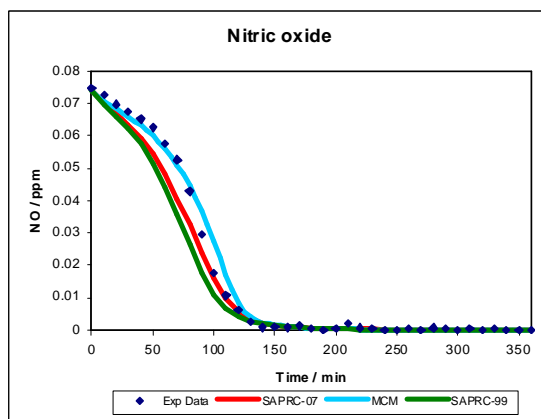
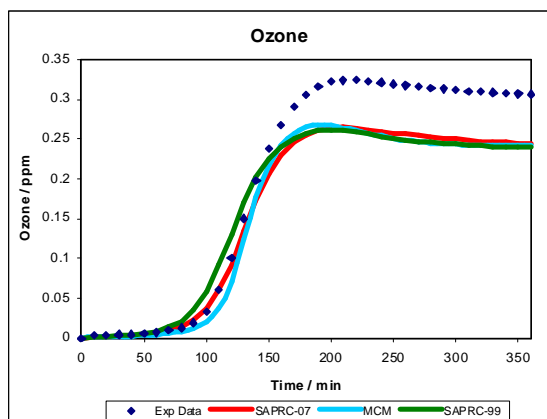


Appendix C1: Modelled results for experiment 303

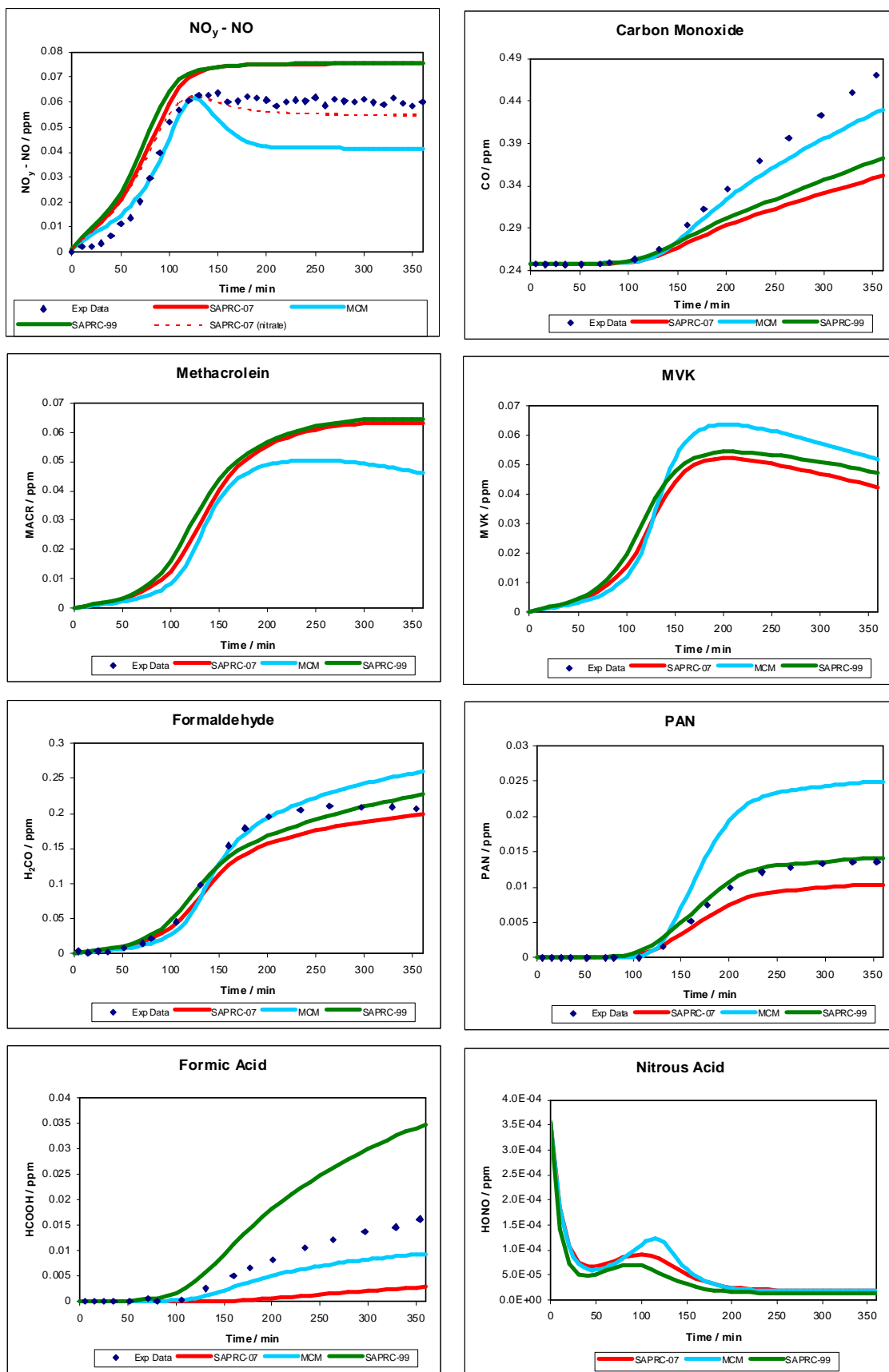


Appendix C1 (cont.): Modelled results for experiment 303

Experiment : 448					
Initial Conditions:			ROC/NO _x	24.00	
NO	74	ppbv	HONO	0.36	ppbv
NO ₂	1	ppbv	J _{NO2}	0.39	min ⁻¹
CO	248	ppbv	HONO gen	0	ppbv hr ⁻¹
Isoprene	360	ppbv	Initial Temp	293.6	°K
CH ₄	1.5	ppmv	Max Temp	305.3	°K
H ₂ O	1169	ppmv	Final Temp	305.1	°K



Appendix C2: Modelled results for experiment 448



Appendix C2 (cont.): Modelled results for experiment 448



Contact Us

Phone: 1 300 363 400

+61 3 9545 2176

Email: enquiries@csiro.au

Web: www.csiro.au

Your CSIRO

Australia is founding its future on science and innovation. Its national science agency, CSIRO, is a powerhouse of ideas, technologies and skills for building prosperity, growth, health and sustainability. It serves governments, industries, business and communities across the nation.